This is to certify that the

thesis entitled

Geochemistry and Origin of the
Yellow Dog Plains Peridotite,
Marquette County, Northern Michigan

presented by

William J. Morris

has been accepted towards fulfillment
of the requirements for

Masters degree in Geology

John T. Wilband
Major professor

Date November 2, 1977

O-7639

11:5864546

JUN 01 2011

GEOCHEMISTRY AND ORIGIN OF THE YELLOW DOG PLAINS PERIDOTITE, MARQUETTE COUNTY, NORTHERN MICHIGAN

By

William J. Morris

A THESIS

Submitted to
Michigan State University
in partial fulfillment of the requirements
for the degree of

MASTER OF SCIENCE

Department of Geology

1977

ABSTRACT

GEOCHEMISTRY AND ORIGIN OF THE YELLOW DOG PLAINS PERIDOTITE, MARQUETTE COUNTY, NORTHERN MICHIGAN

By

William J. Morris

A lower Keweenawan peridotite and several diabase dikes from Marquette County, Michigan, were sampled for comparative analysis. Textures and chemical trends with depth show that the peridotite is a cryptically layered cumulate body. Geophysical data suggests the presence of a zone of massive sulfides, although nickel concentrations in the olivines (> 0.3 percent) suggests that the hypothesized sulfide phase may not be Ni-rich.

The rare earth element (REE) abundances for the peridotite are unusual for an ultramafic rock. This REE distribution is not easily explained by an origin through basaltic fractional crystallization or partial melting with coexisting garnet. Melting in the presence of volatiles may explain the alkali and LRE enrichment of the peridotite. This peridotite probably crystallized from a primary mantle melt within a developing rift zone. The REE distribution for the diabase dikes are consistent with the hypothesis that these dikes may be feeders for Keeweenawan lavas.

ACKNOWLEDGMENTS

Special thanks goes to Dr. John T. Wilband for his advice, enthusiasm and support in every phase of this study. Drs. Thomas A. Vogel and F.W. Cambray critically read the manuscript and made many valuable suggestions. Mr. Vivion Schull provided assistance in the use and operation of the electron microprobe. Dr. Allen M. Johnson of the Institute of Mineral Research drilled the core which was funded by the Michigan Department of Natural Sciences, Geological Survey Division. Mr. David W. Snider allowed use of the drill core in this study and provided many valuable suggestions.

TABLE OF CONTENTS

Page

LIST OF TABLES

LIST OF FIGURES

INTRODUCTION

Few Keweenawan ultramafic rock bodies are exposed in Michigan's Upper Peninsula. At least one relatively fresh and undescribed peridotite outcrops in an area locally known as the Yellow Dog Plains in the northwest sector of Marquette County (Figure 1). Recent paleomagnetic data indicates that the intrusive is lower Keweenawan in age (K. Books, USGS, personal communication, 1976).

The fact that the Yellow Dog Plains peridotite is located in an extensive east-west trending magnetic belt suggests it may be genetically related to exposed similar trending diabase dikes further to the south. These intrusives are apparently related to the Keweenawan rift system as proposed by Chase and Gilmer (1974). This failed continental rift system (Burke and Dewey, 1975) opened slightly around 1.1 billion years ago and resulted in Keweenawan volcanic rocks and associated intrusives.

The presence of the Keweenawan peridotites completes a possible ultramafic to acidic magma series in which a classical differentiation-cumulate model can be ascribed to the origin of the peridotite. In this model the parent is assumed to be basalt. Alternatively, the peridotite could represent a primary mantle melt. These

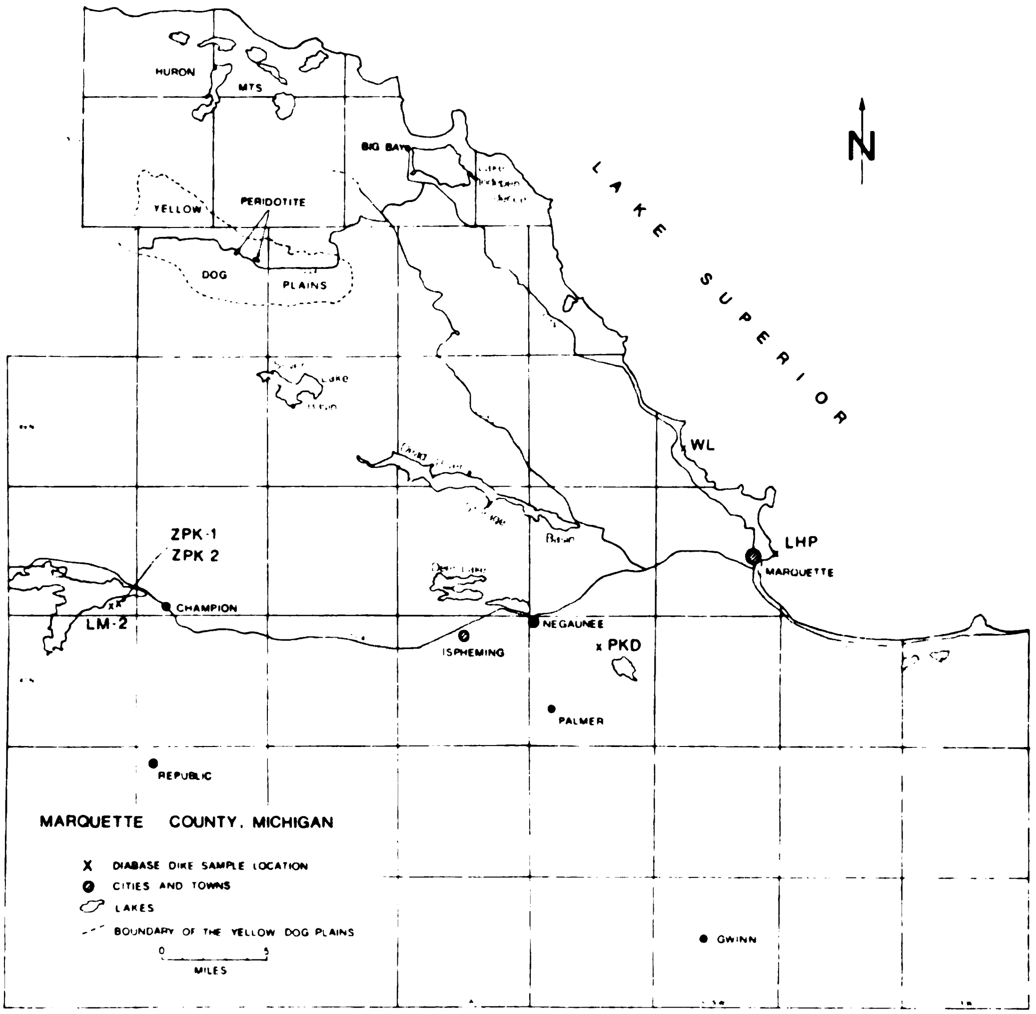

Figure 1.--Marquette county map showing locations of the Yellow Dog Plains Peridotite and sampled diabase dikes.

models are tested by major element and selected trace element geochemistry of whole rock samples of the peridotite body and diabase dikes and of the olivine, clinopyroxene, and orthopyroxenes of the peridotite. The whole rock distribution of selected rare earth elements (REE), La, Ce, Sm, Eu, Yb, and Lu are powerful petrogenetic indicators and are used to evaluate these models for the origin of the peridotite and the diabase dikes.

The concentration of the trace elements Ni, Cr, and Cu were determined from an economic point of view because of the possible association with mineralized Keweenawan rocks, such as the Portage Lake Lava Series (native Cu) and the Duluth Gabbro (Ni-sulfides) and the known association of Ni, Cr, and other precious metals with ultramafic rock bodies. Disseminated sulfides, chalcopyrite and pentlandite, found within the Yellow Dog Plains Peridotite enhance its economic potential.

Geologic Setting

The Yellow Dog Plains Peridotite (YDPP) intrudes the Precambrian X Michigamme slate. It has been dated as lower Keweenawan in age (K. Books, USGS, personal communication, 1976) on the basis of recent paleomagnetic data (reversed polarity). Furthermore, its extreme freshness, and its undeformed nature is evidence that it is younger than the Penokean Orogeny (1.8-2.0 bybp) (Van Schmus, 1976).

Geophysical surveys completed by the USGS (August, 1976) and the Michigan Department of Natural Resources, Geological Survey Division indicate that the YDPP "is part of a dike swarm that extends in a west-northwest direction for about 20 km beneath the Pleistocene drift cover" (Snider et al., 1977). Faulting of the body is suggested by local discontinuities found by this survey.

Keweenawan diabasic intrusions occur in a 70 km wide belt in Gogebic, Iron, Baraga, Dickinson and Marquette counties of Michigan. Within Marquette county these dikes intrude lower Precambrian gneisses and metasedimentary rocks of the Marquette Synclinorium (Gair, 1975; Gair and Thaden, 1968). These dikes invariably trend east-west, have an associated negative magnetic anomaly and are reversely polarized like the peridotite.

The best known middle Keweenawan rocks of Michigan are the Portage Lake Lava Series which are largely tholeiitic basalts with some andesites and minor amounts of rhyolite. The lava series outcrops along the entire length of the Keweenaw Peninsula and is the host for the native copper deposits of Michigan (Figure 2). The volcanic pile lies on the southeast edge of the ancient Keweenaw rift system that is defined by the Mid-continent Gravity High (Chase and Gilmer, 1974).

Hubbard (1975), Green (1972), and White (1972) have determined from geologic and geophysical data that

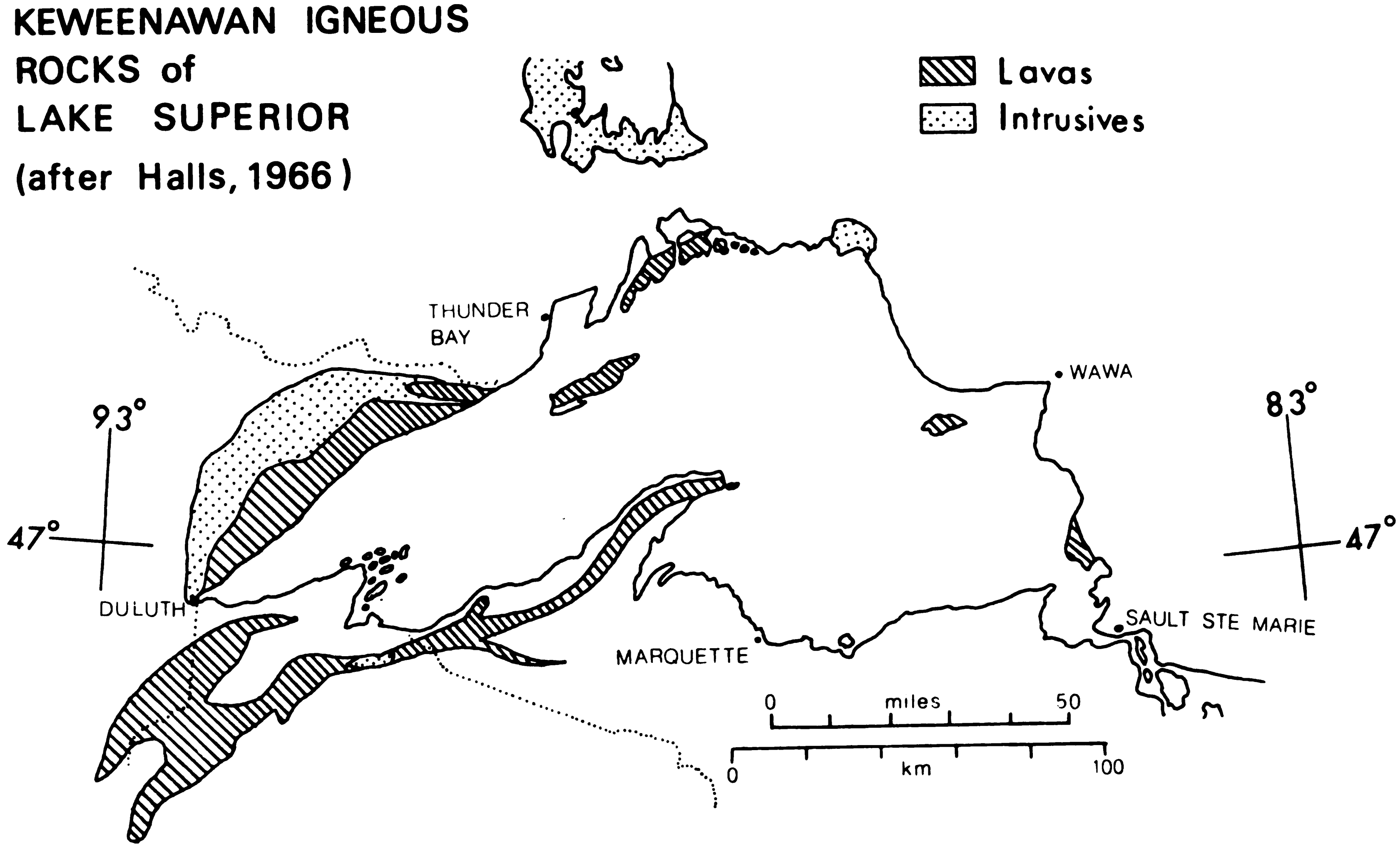

Figure 2.--Keweenawan igneous rocks of the Lake Superior region (after Halls, 1966).

volcanic rocks surrounding Lake Superior were deposited in separate tectonic basins, rather than accumulating during one single event. The paleomagnetic data offers further evidence for separating different basins into lower and middle Keweenawan events. For instance, the middle Keweenawan Portage Lake lavas were thought to extend the entire length of the Keweenaw Peninsula and into northern Wisconsin. Hubbard (1975), however, has shown that volcanic rocks near Ironwood, Michigan are actually lower Keweenawan in age (Powder Mill Group). Green (1972) believes lithic similarities between lower Keweenawan volcanic rocks on the north and south sides of Lake Superior imply that these lavas may have been erupted during the same event and perhaps in a single broad basin.

Paleotectonics

A positive linear Bouguer gravity anomaly extends 1300 km from Lake Superior south to southwest into Kansas (King and Zeitz, 1971). This geophysical gravity anomaly is well known as the Mid-continent Gravity High. Several authors (Chase and Gilmer, 1974; King and Zeitz, 1971) have interpreted this feature as an aborted continental rift system. This rift system may have opened in Keweenawan time approximately 1.1 bybp resulting in the Keweenawan lavas and associated intrusives. Petro (1977) has shown that the suite of Keweenawan rocks does fit into an extensional tectonic setting based on a chemical-type comparison with known extensional rift zones.

Another gravity high that extends southeastward under the Michigan Basin (Hinze et al., 1972) is believed to be an extension of the Keweenaw rift zone. Burke and Dewey (1973) cite this as an example of their plume generated triple junction with the Mid-continent Gravity High, the Michigan Basin anomaly, and the Michipochten area as the three arms of the short-lived Keweenawan spreading center.

Case and Gair (1965) believe that the lower Keweenawan dikes of Michigan were emplaced along a major zone of longitudinal tension fractures of Keweenawan age. Several authors have suggested that these dikes may be feeders for Keweenawan lavas (Wood, 1962; Hubbard, 1975; and others). Dubois (1962) has related lower Keweenawan dikes of Michigan with the Logan sills of Ontario.

Sims and Morey (1972, p. 12) summarize the relationships as follows:

> The close spatial relations of [Keweenawan] rocks of the Duluth Complex, the North Shore Volcanic Group, the Logan Intrusions, and other mafic dike rocks suggest they record a single, but large-scale process of differentiation and intrusion.

Many investigators (Sims, 1976; Burke and Dewey, 1973; Sawkins, 1972; and others) have cited the Keweenawan mineralization of the Duluth Gabbro and Portage Lake Lava

Series as an example of mineralization through tectonic processes.

Location and Description

The YDPP outcrops in two separate locations in the northern section of the Yellow Dog Plains within the Michigamme State Forest. It lies approximately 40 kilometers to the northwest of the city of Marquette, Michigan (Figure 1). The larger roughly oval-shaped exposure outcrops on the north side of county road AAA (location: E½, SW, NW, section 12, T50N, R29W, Champion quadrangle, Marquette county, Michigan) and is 190 meters in length, 120 meters in width, and has a maximum height of 15 meters above the surrounding plains. The smaller exposure is on the south side of county road AAA approximately 800 meters to the WNW of the larger outcrop. It covers an area of only a few square meters at the nose of a hill (location: SW, NW, NW, section 11, T50N, R29W, Champion quadrangle, Marquette county, Michigan).

Topographically, the area surrounding the large exposure is a rather featureless plain mantled by sandy Pleistocene outwash and till. This locally lumbered area is mainly covered by coniferous trees with an underbrush consisting of ferns, mosses, and grasses.

The peridotite, the only rock body exposed in the immediate area, is dark-green to black in color and consists mostly of olivine, clino- and orthopyroxenes and plagioclase feldspar. Sulfide patches up to a centimeter in diameter are present in some hand specimens. The peridotite typically weathers to a light reddish-brown color on exposed surfaces due to the oxidation of iron.

An east-west topographic profile across the center of the body demonstrates its assymmetrical nature. A near vertical cliff of the west end to a height of 15 meters above the surrounding plain and slopes gradually for 170 meters to the level of the plain on the east end. The peridotite is exposed mainly along the west, south, and north flanks of the small hill it defines (Figure 3).

No linear or planar features were observed in the field, other than a north trending fracture zone with dips between 40 and 50^{o}.

Field Techniques: Mapping and Sampling

A north-south, east-west grid system, marked with fluorescent surveyors tape, was established by Brunton compass and metric chain. The grid system was marked off in 30 and 60 meter intervals to adequately cover the outcrop for mapping purposes. Mapping was accomplished by retracing grid lines and mapping the exposures in relationship to the grid lines. Deflection of the compass due to high local concentrations of magnetite caused little problems in continuing straight grid lines since resighting along previous markers was possible.

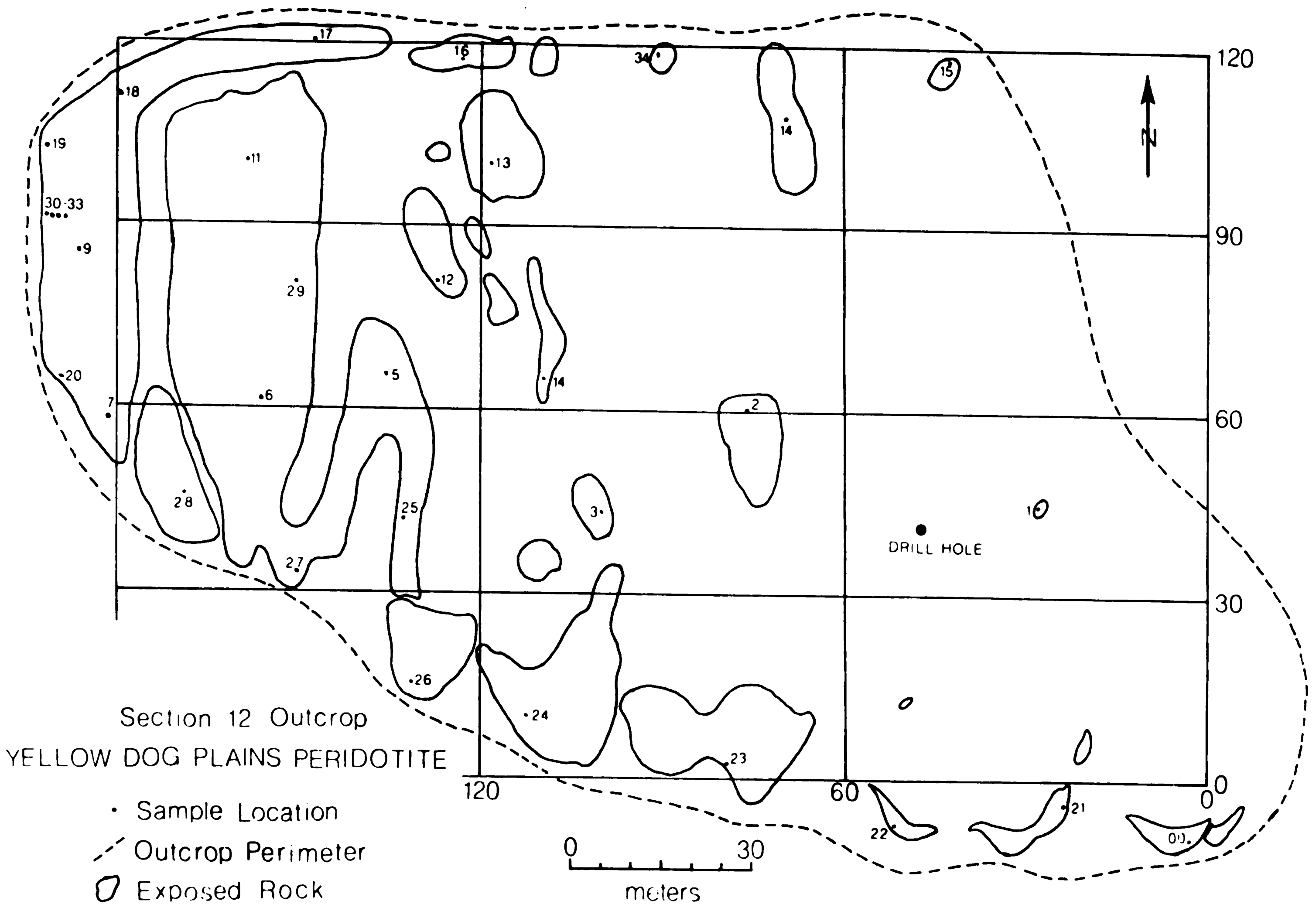

Figure 3.--Field map showing exposure and sampling location on the large outcrop of the peridotite.

The east-west baseline was set parallel to the 235N line of another grid system make by David W. Snider, Michigan Department of Natural Resources, Geologic Survey Division. The north-south baseline coincided with his 700E line. His grid system was used for geophysical work over the peridotite and the surrounding area (Snider et al., 1977), and was tied in with nearby USGS bench marks. Other geophysical survey positions make it possible to relocate this grid system.

After mapping the large exposure, sampling locations (Figure 3) were chosen with the following criteria in mind:

1. along grid intersections
2. along the outcrop perimeter
3. samples showing maximum variability
4. freshness of samples
5. up the west outcrop face
6. adequately spaced over the outcrop.

The maximum height of the outcrop (15 meters) was determined by using the Jacob-staff method (Compton, 1962) with a meter stick and scaling the west face.

In September, 1976, an exploratory drill hole was cored into this body to a depth of 31 meters. Dr. Allan Johnson of the Institute on Mineral Research in Houghton, Michigan, drilled the peridotite for the Michigan Department of Natural Resources, Geologic Survey Division.

The core was turned over to the writer for use in this study.

Several samples of Keweenawan diabase dikes were also collected for analysis and comparison with the YDPP. Their locations represent a wide geographic range as shown in Figure 1. The following table gives a more detailed location for each sampled diabase.

Table 1.--List of diabase dike sample locations.

Sample	Location
WL	NE, SW, SW, section 29, T49N, R25W, Marquette quadrangle, Marquette county, Michigan.
PKD	SE, SW, NE, section 10, T47N, R26W, Palmer quadrangle, Marquette county, Michigan.
LHP	NE, NW, section 24, T48N, R25W, Marquette quadrangle, Marquette county, Michigan, Lighthouse Point sample in city limits.
LM-2	NE, SE, NE, section 35, T48N, R30W, Michigamme quadrangle, Marquette county, Michigan
ZPK-1	NW, SE, NE, section 35, T48N, R30W, Michigamme quadrangle, Marquette county, Michigan.
ZPK-2	SW, SW, NW, section 36, T48N, R30W, Michigamme quadrangle, Marquette county, Michigan.

MINERALOGY

Only minor variation in mineralogy exists between samples of the YDPP, although some rather large sulfide globules up to a centimeter in diameter are found sparingly in hand sample. The peridotite contains up to 50 percent olivine, as much as 35 percent pyroxenes, approximately 10 percent plagioclase feldspar and less than 10 percent opaque minerals.

The range of olivine composition as determined by electron microprobe analysis is Fo_{79-82} (Table 2; Appendix C). Texturely the olivine occurs as sub- to euhedral phenocrysts that commonly share grain boundaries (Figure 4) or are poikilitically enclosed by clinopyroxenes (Figures 5 and 6). This texture implies that the peridotite body is a crystal cumulate. The olivine exhibits various stages of alteration. In some cases they are amazingly fresh (Figure 7) while other olivines are completely altered (Figures 4 and 5). Finely disseminated magnetite is a common alteration product of olivine, and much of the serpentine is psuedomorphic after the olivine. Minor amounts of talc and chlorite are present in some highly altered zones within the peridotite mass.

Table 2.--Average chemical compositions of major elements in minerals of the Yellow Dog Plains Peridotite determined by electron microprobe analysis.

	Olivine (34)	Clinopyroxene (20)	Orthopyroxene (10)
SiO_2	39.00	52.39	54.64
Al_2O_3	n.a.	2.23	1.61
TiO_2	n.a.	.75	.51
FeO	18.15	6.67	11.82
MgO	41.88	17.51	29.00
CaO	.25	18.54	1.86
MnO	.25	.19	.25
Cr_2O_3	.04	.80	.38
NiO	.37	.12	.13
TOTAL	99.94	99.19	100.20

n.a. not analyzed.

Mineral compositional ranges in terms of pure end members.

Olivine $Fo_{79-81}Fa_{19-21}$
Fo = Foresterite (Mg_2SiO_4)
Fa = Fayalite (Fe_2SiO_4)

Clinopyroxene $Wo_{36-41}En_{48-53}Fs_{11}$
Wo=Wollastonite ($CaSiO_3$)
En=Enstatite ($MgSiO_3$)
Fs=Ferrosilite ($FeSiO_3$)

Plagioclase Feldspar $An_{57-65}Ab_{35-43}$
An = Anorthite ($CaAl_2Si_2O_8$)
Ab = Albite ($NaAlSi_3O_8$)

Figure 4.--Euhedral olivine phenocrysts showing cumulate texture. Bottom edge of photograph is 5mm. Plane polarized light. 12M.

Figure 5.--Poikilitic texture of olivine in clinopyroxene. Plane polarized light. 12M.

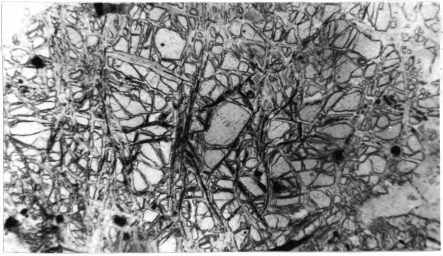

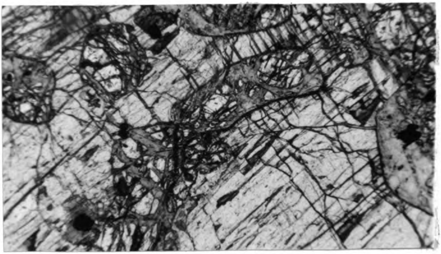

Figure 6.--Poikilitic texture. Note complete psuedomorphic replacement of olivine. Plane polarized light. 4M.

Figure 7.--Euhedral form of a slightly altered olivine phenocryst. Plane polarized light. 6M.

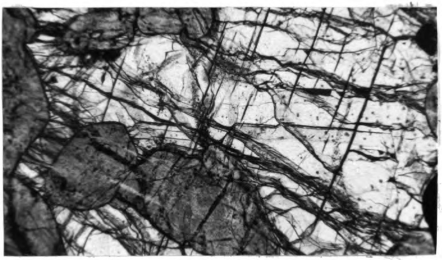

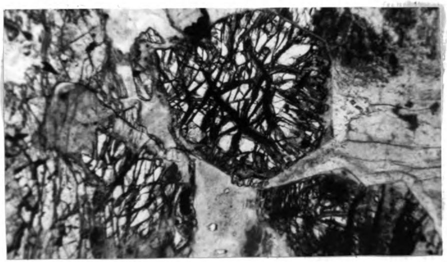

The clinopyroxenes are the next most abundant mineral in the rock (about 25 percent). These augitic clinopyroxenes ($En_{47-54}Wo_{36-41}Fs_{11}$) may be up to a centimeter in diameter and most often poikilitically enclose the forsteritic olivine (Figure 5).

A bronzitic orthopyroxene ($En_{78-80}Wo_{4}Fs_{17-19}$) is also present as an intercumulus mineral. It comprises between 5 and 10 percent of the peridotite. The orthopyroxenes are generally smaller than the clinopyroxene; texturally, they are subhedral and often times intergrown with a clinopyroxene (Figure 8).

The pyroxenes were also analyzed by the electron microprobe, oxide and end-member mineral compositions for each analyzed pyroxene and olivine are listed in Appendix C (averages for each appear in Table 2). Unlike the olivine, the pyroxenes exhibit very little alteration. Most is confined to fractures or cleavage planes. Figure 9 is a triangular diagram showing the compositional separation between coexisting ortho- and clino-pyroxenes.

The plagioclase feldspar grains (An_{57-65}) are elongate in thin section and most often associated with olivine phenocrysts. Intercumulate feldspar (Figure 10), like olivine, exhibits various stages of alteration.

Magnetite is the most abundant opaque mineral present. Other identified opaque minerals includ pyrite, chalcopyrite, pyrrhotite, cubanite, marcasite, bornite,

Figure 8.--Clinopyroxene (pale light) with neighboring subhedral orthopyroxene (dark, left center). X-polars. 8M.

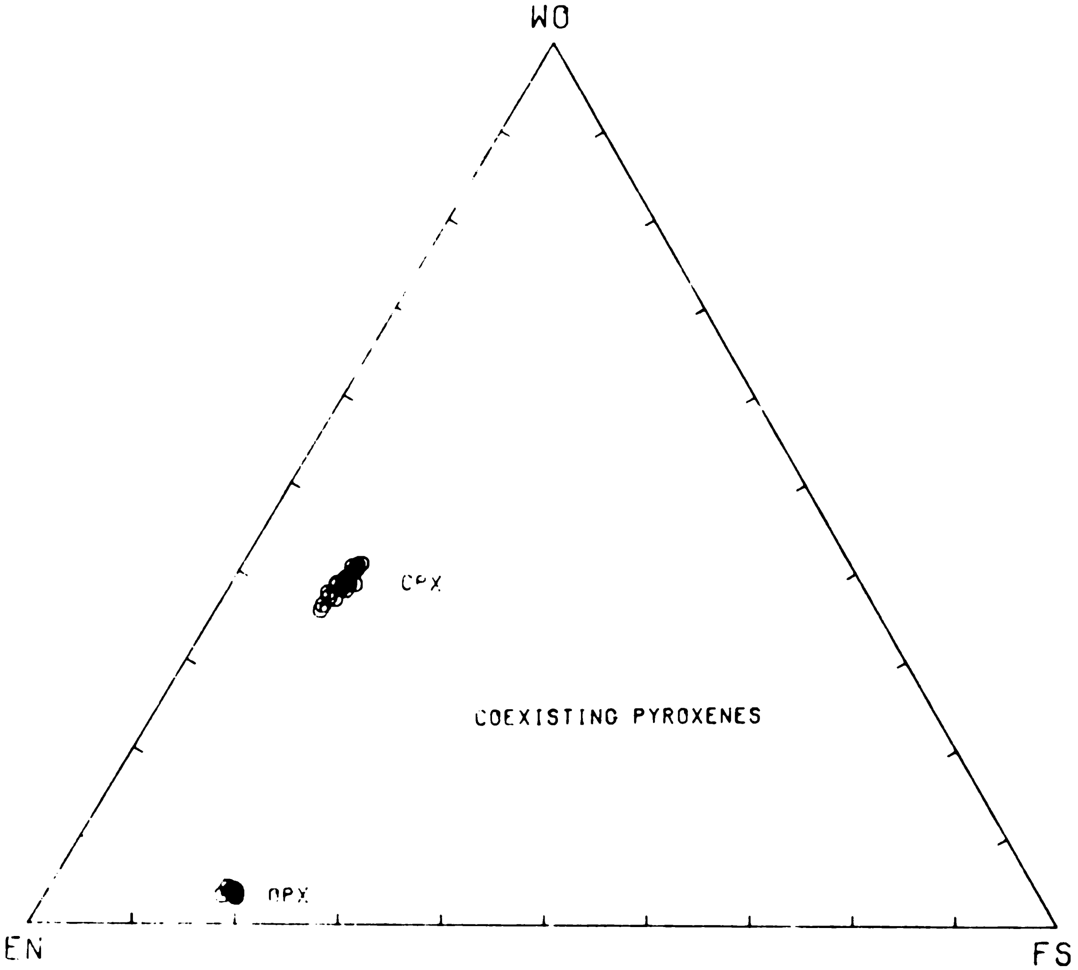

Figure 9.--Triangular diagram showing the compositional separation of coexisting pyroxenes.

Figure 10.--Elongate plagioclase (p) grain showing its intercumulate nature. Adjacent minerals are olivine. Plane polarized light. 12M.

Figure 11.--Sulfide minerals (black) showing globular texture and immiscible relationship. Plane polarized light. YDP-00.

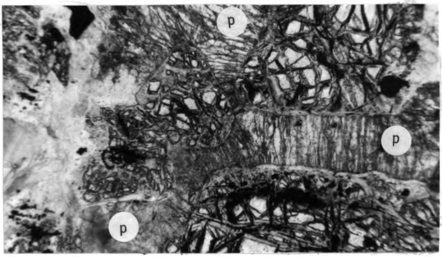
p
p
p

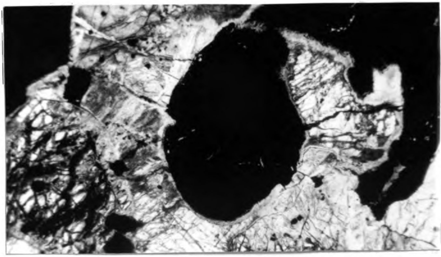

pentlandite, and chromite. Texturally, the sulfide minerals are globular in form and up to a centimeter in diameter. Their globular nature (Figure 11) can be interpreted to indicate that a liquid immiscibility relationship existed during crystallization of the magma. That is, as the silicate magma cooled, it reached the point where it was saturated with respect to sulfide and precipitated an immiscible sulfide liquid (Haughton et al., 1974; Skinner and Peck, 1969). If this immiscible relationship occurred early enough in the crystallization history of the magma and abundant sulfur was present, a massive sulfide zone may have accumulated below the present zone of the peridotite.

If separation by immiscibility occurs, Ni is more highly partitioned toward the sulfide phase (MacLean et al., 1976; Rajamani, 1976). In the peridotite, Ni is concentrated in olivine as opposed to other silicate phases as is expected; and only minor amounts of Ni-sulfides are present in the immiscible sulfide globules. This indicates that olivine crystallized before separation of a sulfide liquid and that any zone of massive sulfides that may be associated with this body is probably Ni-poor.

Other minerals commonly present in minor amounts include biotite, hornblende, and apatite. Biotite is dark-red and strongly pleocroic in thin section and most often associated with magnetite or apatite. Hornblende is light orange in color and exhibits a good amphibole cleavage. Apatite is found in its normal prismatic form associated with biotite or plagioclase, and like biotite is found in all samples.

GEOCHEMISTRY

Major Element

The major element chemistry of the YDPP and the diabase dike samples were determined by X-ray fluorescence analysis, except for Na_2O which was determined by neutron activation analysis and ferrous iron which was determined by titrametric methods. The average whole rock composition for 20 peridotite and seven diabase samples are given in Table 3. The chemical compositions for each analyzed sample is given in Appendix B.

The diabase dike samples represent a wide geographic range (see Figure 1). They are very similar chemically except for some variation in sample PKD. This sample has higher MgO and CaO than the other analyzed diabases and less TiO_2.

The YDPP shows little variation chemically between samples; the largest variations, SiO_2 and MgO, are expected since they comprise nearly 70 percent of the total oxide composition. The relatively high loss on ignition is due to the presence of hydrous alteration minerals such as serpentine, chlorite, and talc. The peridotite may be considered as alkali rich, having higher than normal concentrations of Na, K, and Ca and lower Mg than published

Table 3.--Average whole rock compositions and trace element data for 20 samples of the Yellow Dog Plains Peridotite and 7 samples of diabase dikes.

	Peridotite		Diabase Dike	
		σ		σ
SiO_2	42.44	.91	51.11	1.13
Al_2O_3	4.25	.52	13.85	.73
Fe_2O_3	5.54	.78	3.16	1.01
FeO	8.76	.78	10.00	1.65
MgO	26.20	1.26	6.13	2.98
CaO	4.21	.63	7.78	2.58
Na_2O	.49	.15	2.29	.40
K_2O	.23	.02	1.08	.60
TiO_2	.71	.10	2.14	.92
P_2O_5	.10	.01	.23	.12
MnO	.19	.07	.20	.04
LOI	6.76	.77	2.36	.74
TOTAL	99.88	.77	100.13	1.37
Trace Elements (ppm)				
Mn	1403	149	1536	346
Zn	95	5	102	28
Cu	102	10	118	30
Co	128	8	49	6
Ni	1439	51	60	96
Cr	2565	228	139	101

data for peridotitic rocks (Naldrett and Cabri, 1976; Goles, 1972).

Chemically, the YDPP is similar to komatiites but lack the typical spinifex textures. The $FeO/(MgO+FeO)$ ratio, obtained by normalized oxides after removing LOI and recasting total iron as FeO, was compared to the Al_2O_3 content and found to fall just outside of the komatiite range established by Naldrett and Cabri (1976). Similarly, a plot of MgO versus TiO_2 falls outside the komatiite range. A MgO, CaO, Al_2O_3 ternary plot of the peridotite, however, does fall on the boundary line of the peridotitc komatiite range established by Brooks and Hart (1974).

Figure 12 is an AFM diagram of lower and middle Keweenawan rocks in Michigan showing their general chemical relationships with respect to each other. Similar types of trends of known magma series exist for such bodies as the Skaergaard, Bushveld, and Duluth Gabbro complexes (Tilley, 1950). Although the pattern is similar to a differentiated magma series, the geographic spacing of the samples and the incorporation of lower and middle Keweenawan rocks into the same diagram must be emphasized before a differentiation model is stressed. A chemical mass balance calculation between the lower and middle Keweenawan rocks of Michigan did not confirm that a comagmatic relationship existed between them.

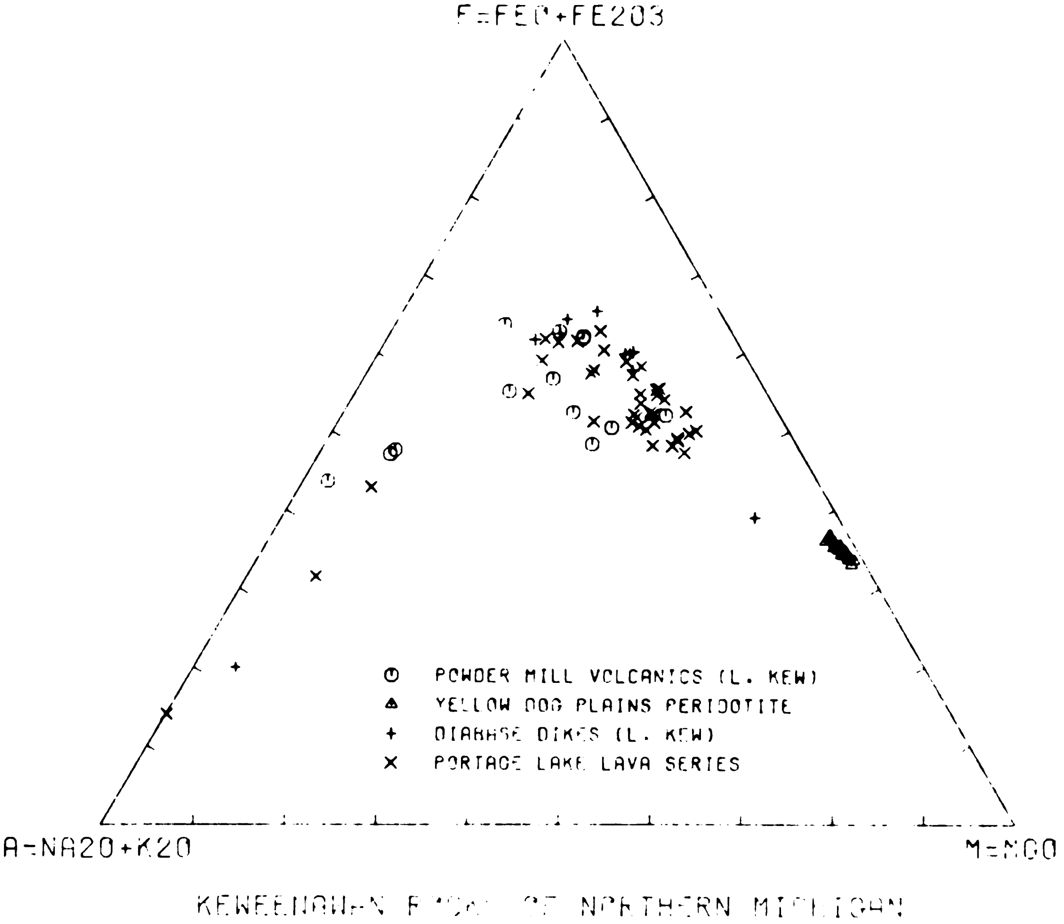

Figure 12.--AFM diagram for lower and middle Keweenawan rocks of Michigan (Powder Mill analyses from Hubbard, 1975; Portage Lake Lava Series analyses from Weis, 1974 and Jolly and Smith, 1972).

Several chemical trends were observed in the drill core. The heavier and more mafic elements, Fe, Mg, Cr, Co, Ni, and Mn, all are more concentrated at depth or have concentration gradients that increase with depth (Figure 13). However, the lighter and more alkalic elements, Al, Ti, Na, and Ca show the opposite trend (Figure 14).

Regular vertical changes in chemical composition are clearly shown by most of the plots of Figures 13 and 14. These chemical trends show that the peridotite is cryptically layered. A common discontinuity in concentration occurs in many of the plots of Figure 15 at a depth of 20 meters, for example, Cr (Figure 15-C), sum of the alkalies (Figure 15-B), Al_2O_3 (Figure 15-D), differentiation index (Figure 15-A), and Na_2O (Figure 15-E). This discontinuity is similar to a cyclic or rhythmic pattern that is commonly found in other more highly layered intrusive rocks, such as the Stillwater, Bushveld, and Sudbury intrusive complexes.

Chemical trends within the olivine and pyroxenes also exist but are not as well established as those cited above. Fe in the olivine decreases with depth (forsterite content increases; Figure 16) as one would expect in a cumulate type body. A correlation coefficient or $r = +0.68$ for Fo with depth was determined for the data. The strongest trend in the pyroxenes is the increase in the

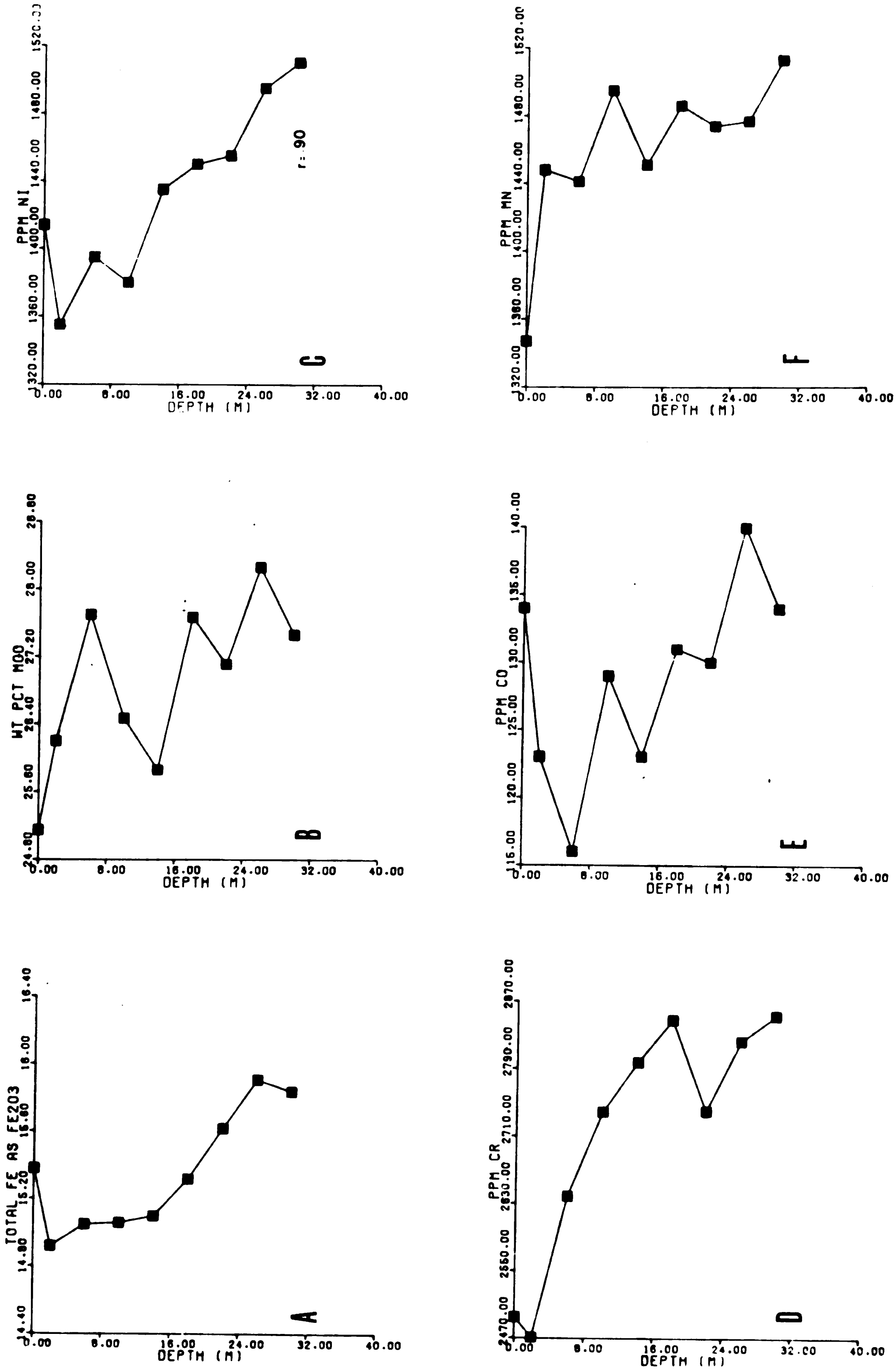

Figure 13.--Whole rock chemical trends increasing with depth.

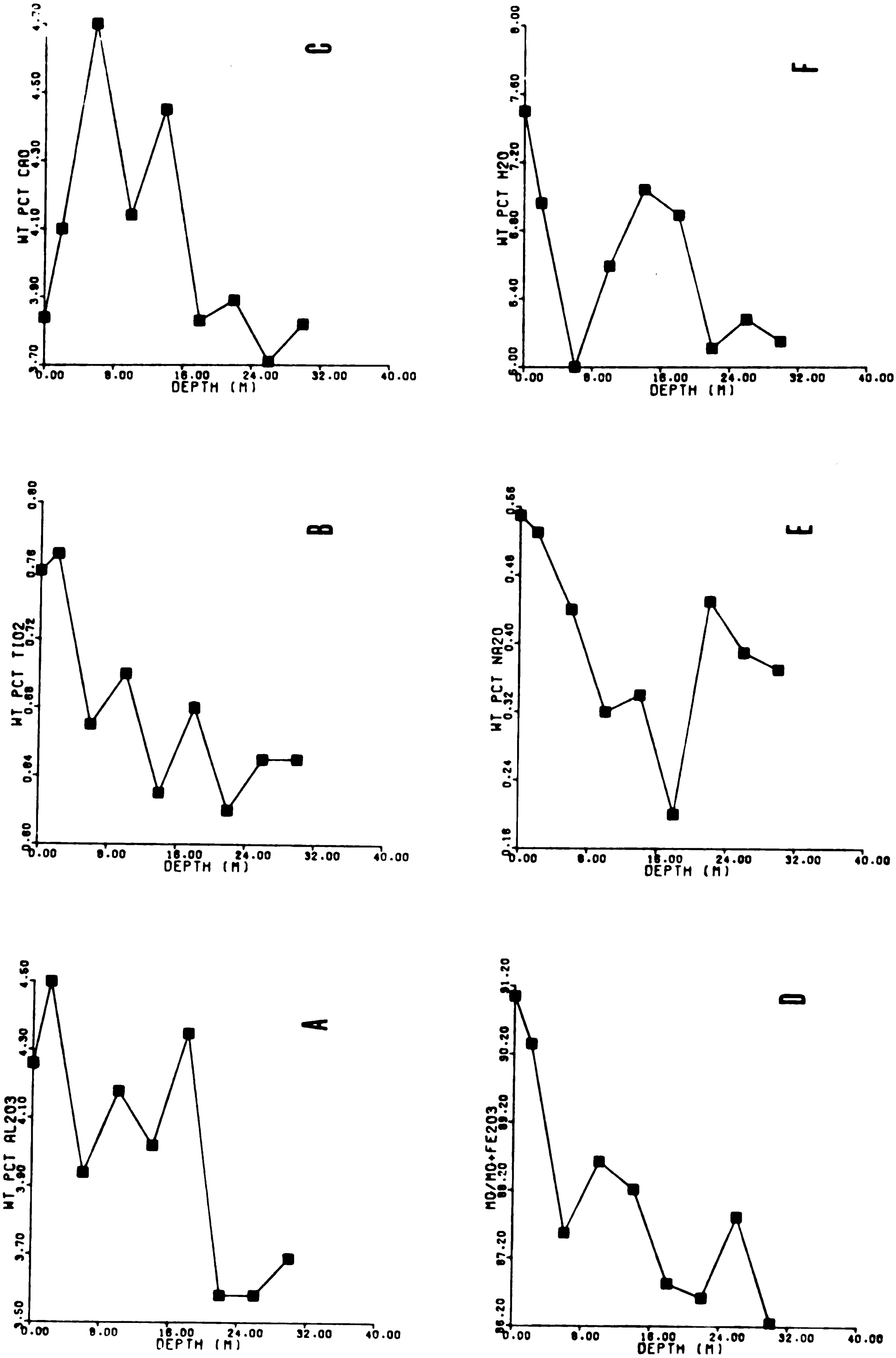

Figure 14.--Whole rock chemical trends decreasing with depth.

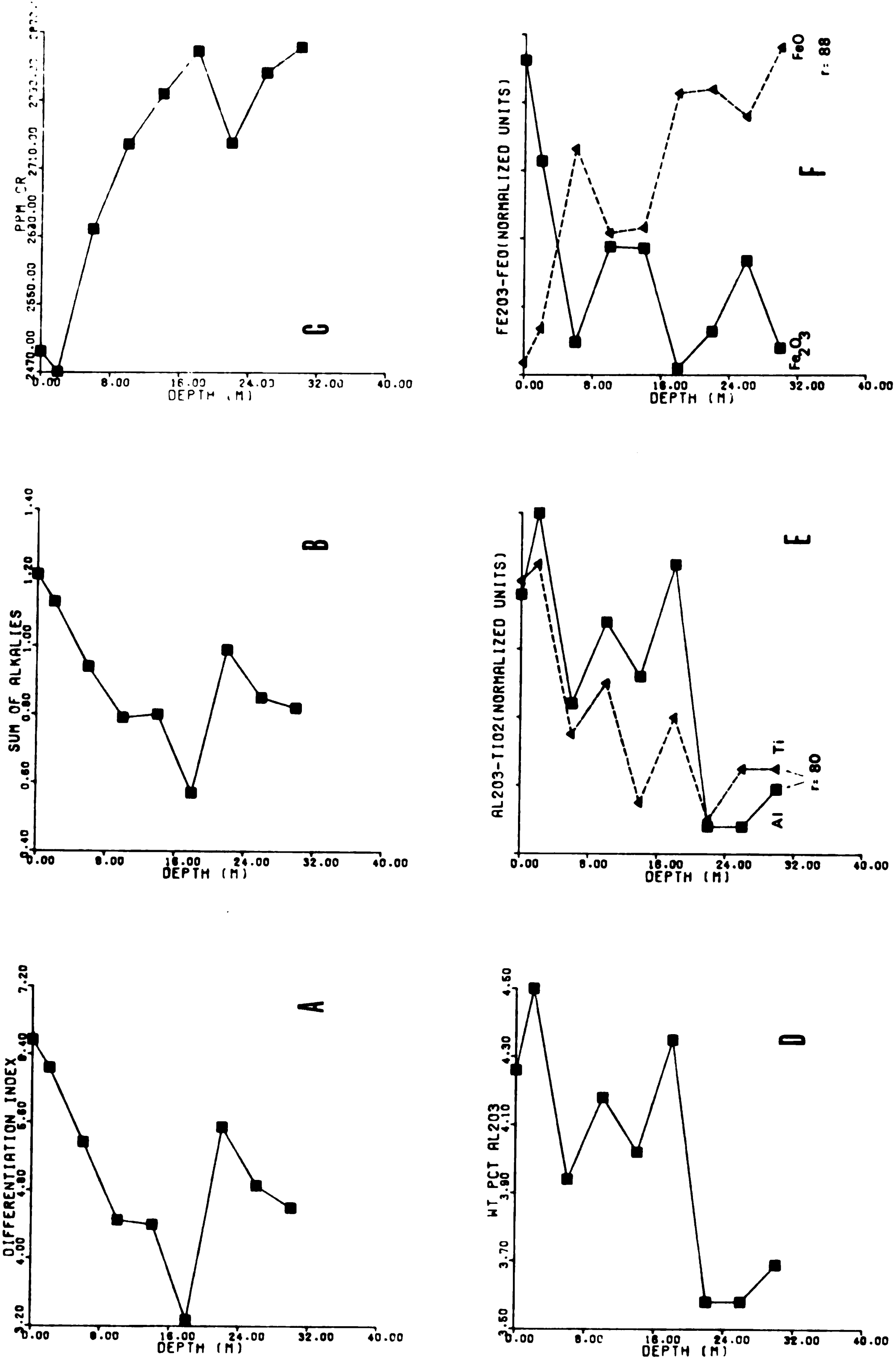

Figure 15.--Whole rock chemical trends with depth exhibiting a cyclic or rhythmic layering.

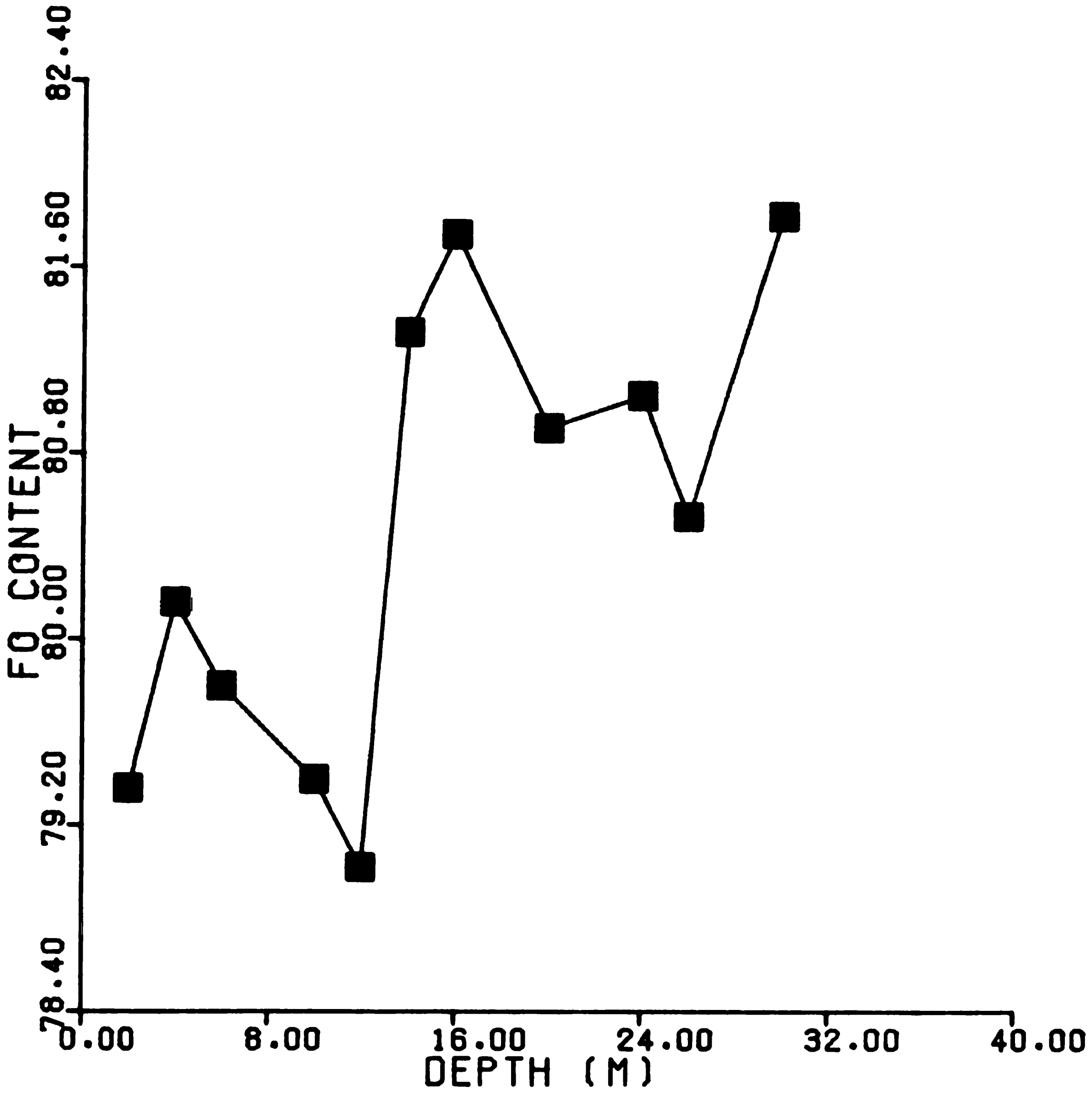

Figure 16.--Plot of olivine forsterite composition versus depth.

concentration of Cr with depth; a weak trend of Ti and Al decreasing with depth is also apparent (see Appendix C). These trends are similar to those of the whole rock analyses.

Trace Element

A logarithmic plot of chondrite-normalized rare earth elements (REE) abundances of the peridotite is shown in Figure 17.

The REE (La, Ce, Sm, Eu, Yb, and Lu) were determined by neutron activation analysis. A relatively large degree of scatter occurs within the light REE of La and Ce (Figure 17 and Appendix B). This scatter may be due to higher concentrations of La and Ce as opposed to the other RE. Frey (1969) observed a scatter of light REE (LREE) in samples of the Lizard peridotite and attributed it to the removal of the LREE from olivine due to serpentinization. Since La and Ce are relatively easy elements to measure by neutron activation analysis, and the precision is good, the scatter is real.

The REE abundances in the peridotite are unusually high when compared with most other ultramafic rocks. As a check on the first analyses the concentrations of the LREE, La and Sm, were redetermined by neutron activation analysis using a combination of liquid and rock powder standards. Both data sets show good agreement (analyses reported in Appendix B).

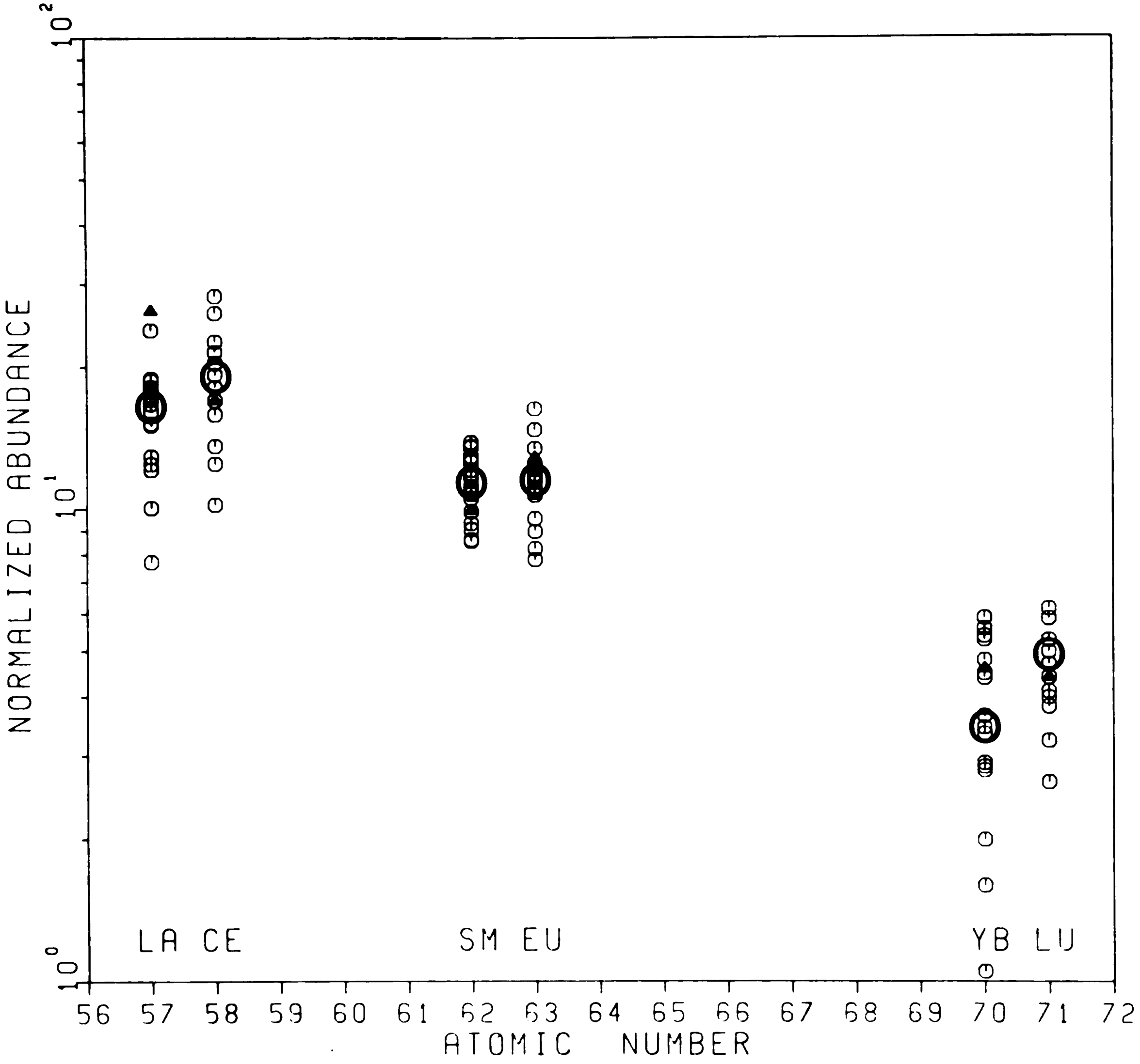

Figure 17.--Comparison of rare-earth element patterns of the Yellow Dog Plains peridotite (octogons = individual analyses; circle = average) and the Duluth Gabbro (average = black triangle).

A definite LRE enrichment pattern is shown in Figure 17. The abundances and trend of the REE was completely unexpected since most ultramafic rocks have a REE abundance less than five times chondritic values and their RE distribution show little if any LREE enrichment pattern. The Yellow Dog Plains peridotite is enriched 15 to 20 times chondritic values for the LREE.

Several lower Keweenawan diabase dike samples were collected and analyzed for comparison with the peridotite and other previously analyzed Keweenawan rocks of northern Michigan. The REE trend for the diabase dikes (Figure 18) show a similar pattern as the YDPP (Figure 17). The diabase dike REE pattern shows a higher LRE enrichment and higher REE concentrations, nearly 50 times chrondritic abundances for the lightest REE.

Except for the LREE abundances, the peridotites trace element concentrations (Table 3; Appendix B) are near the accepted average value for ultramafic rocks (Goles, 1972). Anomalous copper and zinc values do occur. Copper is anomalously high with an average of 100 ppm which is three to four times higher than the average for ultramafic rocks (30 ppm). Zinc in the peridotite is approximately double the average of zinc in ultramafic rocks.

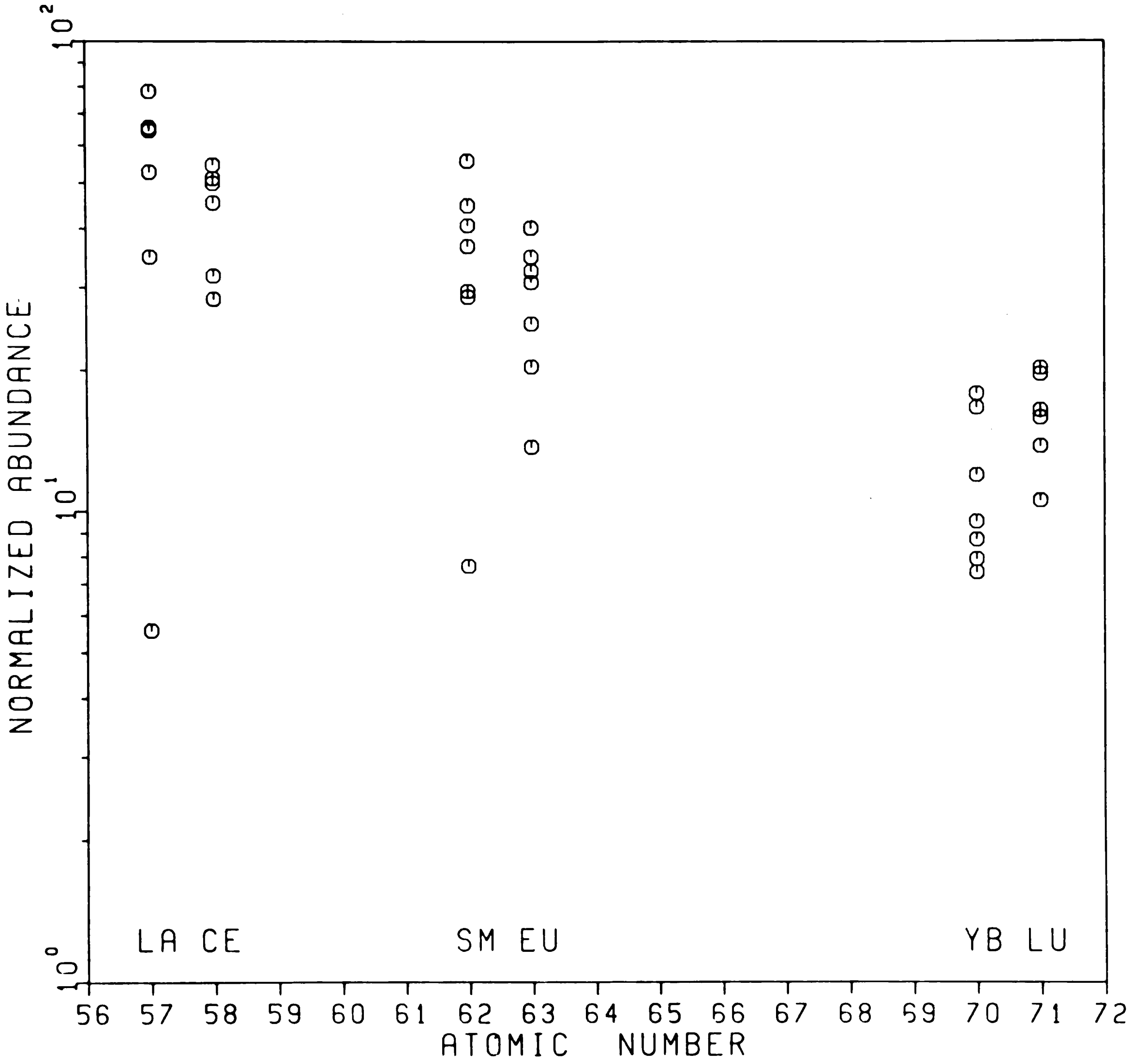

Figure 18.--REE distribution pattern of the sampled diabase dikes.

DISCUSSION

The cyclic cumulate nature of the body is suggested by the variation of Mg, Fe and alkalies with depth and is indicative of a relatively quiescent period in the tectonic cycle. The lack of pervasive serpentinization, and widespread macro- and micro-fracturing which typifies most alpine peridotite masses negates a "solid-state" emplacement model. The origin of the cumulate peridotite, therefore, may be postulated by the following models:

1. The parent liquid was a basaltic melt, generated during rifting followed by crystal settling to yield the peridotite.

2. Deep rifting may have caused local melting of the mantle to form a primary peridotite.

Model 1 has a fundamental appeal if one considers the volumous amount of tholeiitic basaltic lava which accumulated during middle Keweenawan time. A powerful method of testing the viability of this model would be a comparison of RE patterns of ultrabasic cumulates and diabasic rocks of known basaltic parentage with the RE patterns in the investigated peridotite and diabasic dikes. A lack of similarity in RE distributions would confirm the hypothesis stated in model 2 only if a similarity existed between the YDPP and known primary peridotites.

Because of the unusual LRE enrichment in the peridotite the following summary of REE distributions is given so that the two models of the origin for the peridotite can be evaluated.

It is generally believed by most investigators that the REE abundances in the bulk earth are similar to chondritic meteorites and more specifically, that undifferentiated upper mantle rock would be expected to have RE distributions similar to chondrites (Frey, 1969). An investigation by Frey et al. (1968) on basaltic rocks of the Mid-Atlantic Ridge has substantiated this hypothesis. These oceanic tholeiites or sub-alkaline ridge basalts can be distinguished from the LREE enriched continental basalts and alkali basalts of oceanic islands. Frey (1969) notes that this enrichment appears to occur during generation of these magmas within the upper mantle. Furthermore, he states that

> ....residual material left after basalt formation would be expected to have RE abundances ranging from nearly chondritic distributions to light RE depleted distributions (p. 354).

Philpotts et al. (1972) have shown that cumulate peridotites with low concentrations are consistent with fractional crystallization from a liquid with tholeiitic

REE concentrations. Therefore ultrabasic residual rocks, or peridotite cumulates derived from tholeiitic basalts should have RE distributions as generalized in Figure 19, Curve A. This pattern would be expected for the YDPP if it originated by a fractional crystallization model (model 1). The trends shown in Figure 19 represent those expected for various differentiated fractions of a primary basaltic melt. The cumulate ultramafic (Curve A) is LRE depleted or has a near chondritic abundance, whereas successively less basic fractions are more enriched in the LREE (Curves B and C).

The REE's in most rocks are contained in the high Na, K, and Ca minerals (Frey, 1970), mainly the amphiboles, feldspars, and most alkali and silica rich minerals. Olivine, orthopyroxenes, and garnet generally favor the incorporation of the heavier RE's. Thus, the LREE's should be more concentrated in the intercumulate phases of the peridotite. The REE abundances in the separate mineral phases have not been determined. These REE's could be helpful for further interpretation for the origin of the peridotite. The averaged whole rock chondrite-normalized abundances for the peridotite and other basic and ultrabasic rocks for which their origin is known are presented in Figure 20.

The trends in Figure 20 show the expected depletion of the LREE or chondritic REE pattern for cumulate

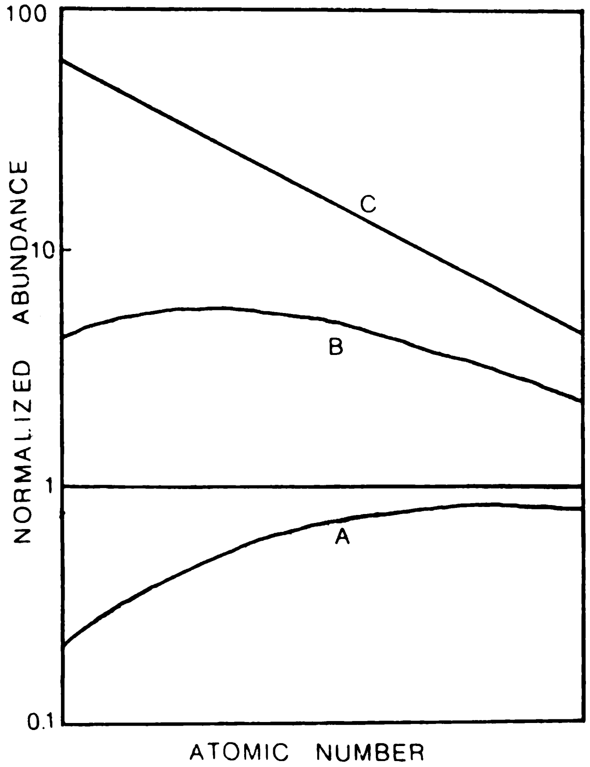

Figure 19.--REE trend for a fractional crystallization model of a basaltic magma.
A = first crystallate
B = solid to crystallizing in equilibrium with the liquid
C = last residual liquid after fractional crystallization.
(Schilling and Winchester, 1966)

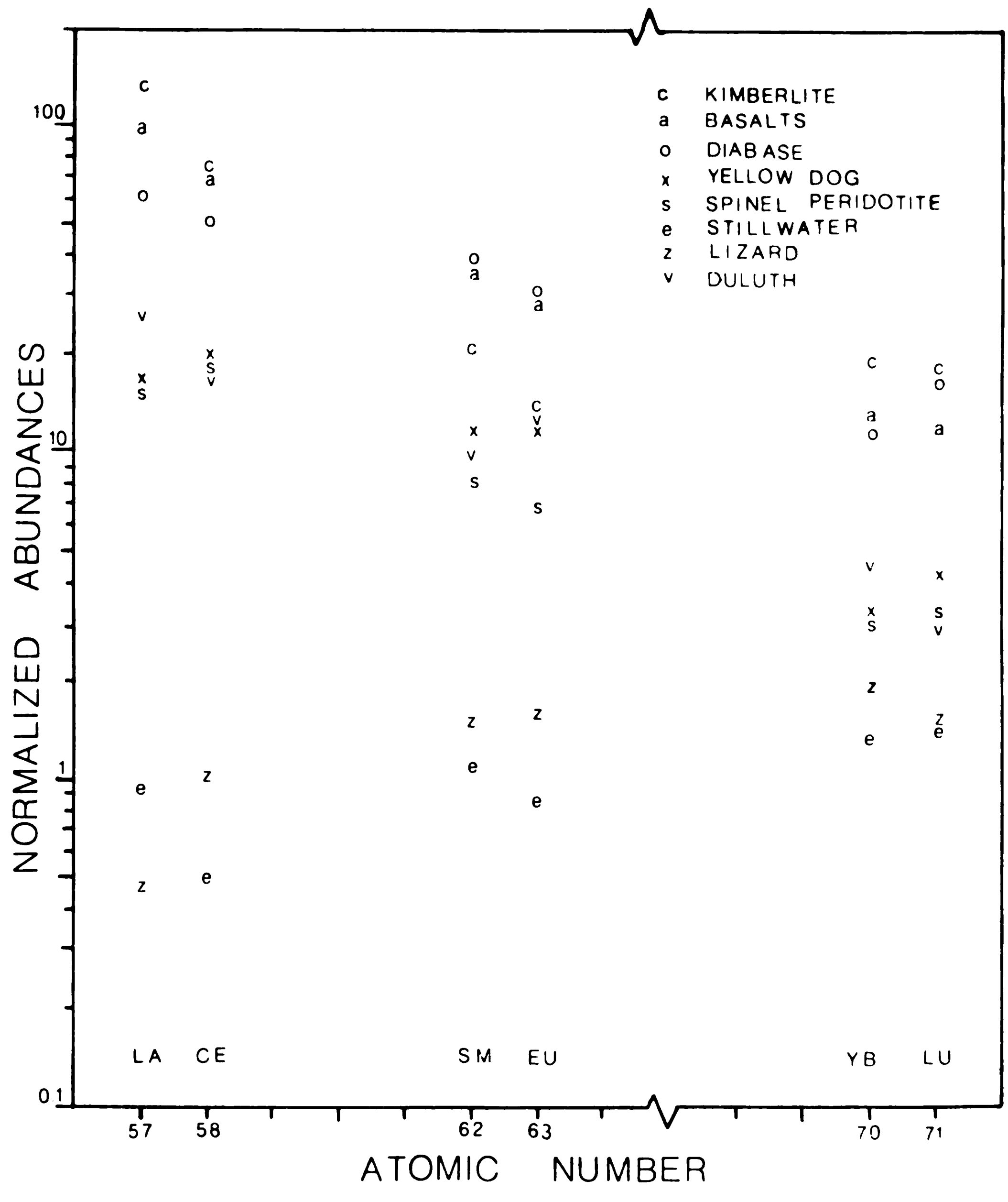

Figure 20.--Chondrite normalized REE abundance patterns for several basic and ultrabasic rocks.

ultramafics from the Stillwater complex, which is similar to those for the Bushveld and Muskox complexes, all of which represent cumulates from a primary basalt liquid (model 1). This trend is not observed in the Yellow Dog Plains peridotite, which shows a relatively strong LREE enrichment. Data in Table 4 further illustrate this enrichment, particularly by comparison of the La/Yb ratios of these ultramafics to the La/Yb ratio of the investigated peridotite.

Kimberlites show a high LREE enrichment pattern, with high La/Yb ratios of 12 to 167 (Frey et al., 1971; Paul et al., 1975). The extreme enrichment is thought to be due to the high volatile content and the association of alkalic rocks with kimberlites which are known to concentrate the LREE's. Paul et al. (1975) believes RE abundances in Indian kimberlites are consistent with a derivation by partial melting of a hydrous garnet peridotite, followed by fractional crystallization of the magma.

An unusual fact about the Yellow Dog Plains peridotite is that it has a REE trend and La/Yb ratios which are similar to some gabbroic rocks such as those from the Duluth Gabbro and the Skaergaard intrusion (Figure 20). If the peridotite was a cumulate differentiate from a gabbroic parent it would not retain the same REE distribution of that magma, but should have lower REE concentrations than those observed. Therefore the

Table 4.--REE in some basic and ultrabasic rocks.

Rock	La	Ce	Sm	Eu	Yb	Lu	La/Yb
Yellow Dog Plains peridotite (20)	5.37	16.2	2.11	.80	.65	.16	8.26
St. Paul's Rock[d] spinel peridotite (3)	5.0	15.3	1.50	.47	.71	.11	7.04
Duluth[e] Gabbro (1)	8.7	15	1.80	.89	.92	.15	9.46
Stillwater[a] peridotite (1)	.31	.44	.20	.059	.27	.05	1.1
Lizard[d] peridotite (2)	.01	.02	.11	.045	.33	.045	0.3
Alpine[b] peridotite (Alps) (6)		.201	.154	.067		.28	
Peridotitic[c] komatiite (1)	.82	2.3	.58	.21	.49	.08	1.7
Kimberlite[a] (1)	43	66	3.76	.86	3.75	.55	12
Keweenawan diabase dikes (7)	19.9	45	7.14	2.12	2.29	.55	8.7
Composite[e] Continental Basalts (282)	31.9	59	6.58	1.87	2.61	.42	12.2
Chondrites[e] (9)	.330	.88	.181	.069	.200	.034	1.65

Number in parentheses represent the number of published analyses used to determine the above REE abundances. Data taken from:

[a] Frey et al., (1971).

[b] Loubet et al., (1975).

[c] Hermann et al., (1976).

[d] Frey, (1970).

[e] Frey et al., (1968).

observed REE distribution of the peridotite is not easily explained by a fractional crystallization model from a basaltic magma. The pattern for the diabase dikes, however, is similar to those of primary basaltic rocks derived by mantle melting and may further support the hypothesis that the diabase dikes are feeders for the Keweenawan basaltic rocks of Northern Michigan.

A possible explanation for the REE pattern is contamination of the peridotite by assimilation of crustal rocks which are enriched in the LREE's. The relatively uniform chemistry, mineralogy, and the absence of xenoliths in the peridotite seem to negate this as a possible explanation.

The YDPP, like some spinel peridotites, of St. Paul's Rocks are highly potassic ($>$ .11 percent K_2O); both exhibit a similar LREE enrichment pattern (Figure 20) and have higher concentrations of Ce than La relative to chondrites. Frey (1970) believes that REE trends in high K rocks peak at Ce whereas in low K rocks ($<$ .11 percent K_2O) La is the more enriched RE.

The St. Paul's Rocks are a group of islets near the axis of the Mid-Atlantic Ridge, 80 km north of the equator. This area is one of considerable tectonic activity and there has been considerable discussion pertaining to the possible relationship of these rocks to the oceanic upper mantle. Wyllie (1967) suspects that considerable amounts of volatiles accompanied the emplacement of this peridotite. The K rich peridotites may represent undifferentiated upper mantle material and K poor peridotites may be representative of residues left after basalt generation (Frey, 1970; Tilley, 1966). None of the spinel peridotites have RE patterns expected for unidfferentiated mantle material (Frey, 1970).

Frey (1970) cites two mechanisms for generation of a LRE enriched ultramafic rock within the mantle: (1) an ultramafic liquid with chondritic RE abundances coexisted with several ultramafic minerals (garnet, olivine, and orthopyroxene) which have distribution coefficients favoring the heavy REE (HREE), or (2) a peridotitic ultramafic rock accumulated from a light RE enriched partial melt of mantle material. In either model the source magma must be enriched in the light REE (LREE) or there is a component of differentiation which is LRE deficient.

In order to generate a LRE enriched peridotite by mechanism 1, Frey (1970) assumes that a mantle melt crystallized small amounts of olivine, orthopyroxene, and particularly garnet as it moved upward, all of which favor the incorporation of HREE. The lack of garnet in the St. Paul's Rocks and the inability of this process to explain the alkali enrichment relative to mantle concentrations reduce the viability of this mechanism as a model for the enrichment of LRE and large ion lithophile elements (LILE) in the peridotites. Frey favors the second mechanism and hypothesizes that the partial melt is an alkali basalt. The peridotite accumulated at depth from the basalt parent. He shows that the REE concentrations of the St. Paul's peridotites are in equilibrium with such a liquid by Shaw's (1970) mass balancing equations.

If this mechanism is applied to the YDPP, the presence of alkali basalt is required. No such rocks are known to exist in the geographic region. Furthermore, if a Keweenawan diabasic melt was the parent it would be expected to have approximately 120 times chondritic abundances for the LREE, if the melt was in equilibrium with a peridotite, based on Shaw's mass balance equations. These REE calculations (Table 5) show that there is no apparent comagmatic relationship between the YDPP and the lower Keweenawan diabase dikes. If the peridotite was a residual of a fractionally crystallized melt, the abundance of plagioclase suggests that a positive Eu anomaly should occur; it does not. Thus, neither of Frey's mechanisms for generating a LRE enriched ultramafic rock seem to adequately explain the LRE and LILE enrichment in the YDPP.

Eggler (1976) and Newton and Sharp (1976) argue that volatiles are likely to be bound in minerals rather than in a vapor phase in the continental upper mantle

Table 5.--Theoretical REE abundances determined by Shaw's mass balance equations. For a diabasic liquid in equilibrium with a solid having the YDP peridotites REE concentrations, and the predicted REE concentration for the peridotite in equilibrium with a liquid that has the analyzed REE abundances of the diabase dikes.

	Diabase Melt	Chondrite Normalized	Predicted Peridotite	Chondrite Normalized
La	45	137	1.17	3.5
Ce	104.5	119	3.08	3.5
Sm	7.1	39	0.60	3.3
Eu	2.4	35	0.26	3.7
Yb	1.1	5.5	0.32	1.6
Lu	0.26	7.6	0.096	2.8

compared with the oceanic mantle. Mysen and Holloway (1977) state that a two or more component vapor phase in the oceanic upper mantle may

> ....vary the trace element content and the relative enrichment of the rare earth elements in the upper mantle on a regional scale.

The lack of partition coefficients between multicomponent vapors and condensed silicates (liquid and crystals), limit a quantitative evaluation of the effects of a vapor phase (Mysen and Holloway, 1977).

The importance of volatiles in the distribution of trace elements has been stressed by many investigators. Mysen and Kushiro (1976) found that melting of peridotite in the absence of volatiles is nearly isobarically invariant whereas other investigators have shown that melting of peridotite + H_2O + CO_2 is at least divariant. Mysen and Holloway (1977) experimentally determined that the REE pattern of an alkali basalt liquid generated by about 2 percent partial melting of a volatile free peridotite mineral assemblage of olivine, clinopyroxene, orthopyroxene and spinel does not have an REE pattern of natural alkali basalts. They therefore concluded that alkali basalt coult not be generated by direct partial melting of any kind of a volatile-free peridotite upper mantle source. Although alkali basalt is not present in the region the fact that REE distributions are apparently controlled by volatiles is an important point to bear in mind with respect to the origin of the YDPP.

The importance of volatiles in enriching kimberlites in the LREE was previously mentioned. The origin of kimberlites is attributed to ascending local primary mantle melts rich in volatiles. Shimizu's (1974) investigation of peridotite nodule REE patterns presents evidence that the mantle is heterogeneous. Mysen and Holloway (1977) suggest that trace element fractionation of the upper mantle can be of a temporary nature and probably quite localized geographically.

Any model for the origin of YDPP must account for the unusual REE distribution pattern and the high alkali abundances. The peridotite is believed to represent crystallization of a peridotite liquid that was generated within the mantle, in a developing rift and emplaced into the crust along a linear zone. Because of the presence of plagioclase the depth of crystallization was above the eclogite transition zone. The unusual trace element characteristics of the YDPP could result from localized melting of a heterogeneous portion of the upper mantle rich in volatiles which generated a peridotitic liquid rich in the LREE and the LILE.

CONCLUSIONS

The YDPP is a lower Keweenawan ultramafic body that outcrops in the northern Peninsula of Michigan. Recent geophysical data (Snider et al., 1977) indicates that the peridotite is an east-west elongate body, at least 1.5 km long. Other geophysical data, known Keweenawan mineralization, anomalous Cu concentrations, and the presence of immiscible sulfides are all possible indicators that the peridotite may be economically important. The high concentration of Ni in olivine as opposed to sulfide minerals suggest that a hypothesized sulfide zone is not Ni rich.

Mineralogically, the peridotite contains approximately 50 percent olivine, 35 percent pyroxenes, 10 percent plagioclase feldspar, and 5 percent opaque minerals. Chemically, the peridotite is alkali-rich with higher K, Na and Ca and lower Mg concentrations than other ultramafic rocks. Textural features and regular chemical changes with depth provide evidence that the peridotite is a cryptically and possibly rhythmically layered cumulate body.

The REE distribution pattern for the peridotite is enriched in the LREE, which is highly unusual for an ultramafic rock. Interpretation of this LREE enrichment is not readily explained by fractional crystallization of a basaltic magma. The YDPP has a similar REE distribution pattern to spinel peridotites from St. Paul's Rock. Although the origin for the spinel peridotites is not applicable to the YDPP. It is suggested that the YDPP originated from a primary mantle melt enriched in the LRE and the alkali elements. A volatile rich phase must have existed in order to explain this unusual enrichment. Emplacement of this ultramafic melt into the crust can be explained by continental rifting during Keweenawan time.

Chondrite normalized REE data of the diabase dikes, also LRE enriched, is consistent with an origin by fractional crystallization of a basaltic magma. This REE pattern may support the hypothesis that these dikes are feeders for the Keweenawan volcanic rocks of Northern Michigan.

REFERENCES

REFERENCES

Brooks, C. and Hart, S.R. 1974. On the significance of Komatiite: Geology, 2, 107-110.

Burke, K. and Dewey, J.F. 1973. Plume generated triple junctions: Key indicators in applying plate tectonics to old rocks: Jour. Geology, 81, 406-433.

Case, J.E. and Gair, J.E. 1965. Aeromagnetic map of parts of Marquette, Dickinson, Baraga, Alger and Schoolcraft Counties, Michigan, and its geologic interpretation: U.S. Geol. Survey Geophys. Inv. Map GP-467.

Chase, C.G. and Gilmer, T.H. 1973. Precambrian plate tectonics: The Mid-continent Gravity High: Earth planet. Sci. Lett., 21, 70-78.

Compton, R.R. 1962. Manual of Field Geology: John Wiley and Sons, New York, 378p.

Dubois, P.M. 1962. Paleomagnetism and correlation of Keweenawan rocks: Canada Geol. Survey Bull., 71, 75p.

Eggler, D.H. 1976. Does CO_2 cause partial melting in the low-velocity layer of the mantle?, Geology, 2, 69-73.

Fabbi, B.F. 1971. Rapid x-ray fluorescence determination of Phosphorus in geologic samples: Appl. Spectrosc., 25, 41-43.

________. 1972. A refined fusion x-ray fluroescence technique and determination of major and minor elements in silicate standards: Amer. Mineral., 57, 237-245.

Flanagan, F.J. 1973. 1972 values for international geochemical reference samples: Geochim. Cosmochim. Acta, 37, 1189-1200.

________. 1969. Rare earth abundances in a high temperature peridotite intrusion, Geochim. Cosmochim. Acta, 33, 1429-1447.

Frey, F.A. 1970. Rare earth and potassium abundances in St. Paul's Rock, Earth Planet. Sci. Lett., 7, 351-360.

Frey, F.A., Haskins, L.A. and Haskins, M.A. 1971. Rare-earth abundances in some ultramafic rocks: Jour. Geophys. Res., 76, 2057-2070.

Frey, F.A., Haskins, M.A., Poetz, J.A. and Haskins, L.A. 1968. Rare-earth abundances in some basic rocks: Jour. Geophys. Res., 73, 6085-6098.

Gair, J.E. 1975. Bedrock geology and ore deposits of the Palmer quadrangle, Marquette County, Michigan: U.S. Geol. Survey, Prof. Paper 769, 159p.

Gair, J.E. and Thaden, R.E. 1968. Geology of the Marquette and Sands quadrangles, Marquette County, Michigan: U.S. Geol. Survey, Prof. Paper 397, 77p.

Goles, G.C. 1967. Trace elements in ultramafic rocks, in Wyllie Ied.), Ultramafic and Related Rocks, John Wiley and Sons, New York, 352-362.

Gordon, G.E., Randle, R., Goles, G.G., Corliss, J.B., Beeson, M.H. and Oxley, S.S. 1968. Instrumental activation analysis of standard rocks with high-resolution γ-ray detectors: Geochim. Cosmochim. Acta, 32, 369-396.

Green, J.C. 1972. General geology Northeastern Minnesota, in Sims, P.K. and Morey, G.B. (eds.), Geology of Minnesota: A Centennial Volume, Minn. Geol. Survey, 292-293.

Halls, H.C. 1966. A review of the Keweenawan Geology of the Lake Superior region: Amer. Geophys. Union, Monograph 10, 3-27.

Haskins, M.A. and Haskin, L.A. 1968. REE in the Skaergaard, Geochim, Cosmochim Acta, 32, 433-447.

Haughton, D.R., Roeder, P.L. and Skinner, B.J. 1974. Solubility of Sulfur in mafic magmas: Econ. Geol., 451-467.

Hermann, A.G., Blanchard, B.P., Haskins, L.A., Jacobs, J.W., Knake, D., Korotev, R.L. and Brannon, J.C. 1976. Major, minor, and trace element compositions of peridotitic and basaltic komatiites from the

Precambrian crust of Southern Africa, Contrib. Mineral. Petrol., 59, 1-12.

Hinze, W.J., Roy, R.F. and Davidson, D.M. 1972. The origin of late Precambrian rifts (abs): Geol. Soc. Amer. Abstracts with Programs, 4, 723.

Hubbard, H.A. 1975. Lower Keweenawan volcanic rocks of Michigan and Wisconsin: U.S. Geol. Survey, Jour. Res., 3, 529-541.

Jolly, W.T. and Smith, R.E. 1972. Degradation and metamorphic differentiation of the Keweenawan tholeiitic lavas of Northern Michigan, U.S.A.: Jour. Petrology, 13, 273-309.

King, E.R. and Zietz, I. 1971. Aeromagnetic study of the Mid-continent Gravity High of the Central U.S., Geol. Soc. Amer. Bull., 82, 2187-2207.

Loubet, M., Shimizu, N. and Allegre, C.J. 1975. REE in alpine peridotites, Contrib. Mineral. Petrol., 53, 1-12.

MacLean, W.H. and Shimazaki. 1976. The partition of Co, Ni, Cu, and Zn between sulfide and silicate liquids, Econ. Geol., 71, 1049-1057.

Mysen, B.O. and Holloway, J.R. 1977. Experimental determination of rare earth fractionation patterns in partial melts from peridotite in the upper mantle, Earth. Planet. Sci. Lett., 34, 231-237.

Mysen, B.O. and Kushiro, I. 1976. Compositional variations of coexisting phases with degree of melting of peridotite in the upper mantle, Am. Mineral. in press.

Naldrett, A.J. and Cabri, L.J. 1976. Ultramafic and related mafic rocks: Their classification and genesis with special reference to the concentration of nickel sulfides and the platinum-group elements: Econ. Geol. 71, 1131-1158.

Newton, R.C. and Sharp, W.E. 1975. Stability of forsterite $+CO_2$ and its bearing on the role of CO_2 in the mantle, Earth. Planet. Sci. Lett., 26, 239-248.

Paul, D.K., Potts, P.J., Gibson, I.L. and Harris, P.G. 1975. RE abundances in Indian kimberlites, Earth Planet. Sci. Lett., 25, 151-158.

Petro, W.L. 1977. Major element chemistry and tectonic setting of plutonic rock suites: M.S. Thesis, Michigan State University, 52p.

Philpotts, J.A., Schnetzler, C.C. and Thomas, H.H. 1972. Petrogenetic implications of some new geochemical data on ecologitic and ultrabasic intrusions, Geochim. Cosmochim. Acta, 36, 1131-1166.

Phinney, W.C. 1970. Chemical relations between Keweenawan lavas and the Duluth Complex, Minnesota: Geol. Soc. Amer., 81, 2487-2496.

Rajamani, V. 1976. Distribution of iron, cobalt and nickel between synthetic sulfide and orthopyroxene at 900°C, Econ. Geol., 71, 795-802.

Reynolds, R.C. 1963. Matrix corrections in trace element analysis by x-ray fluorescence: estimation of the mass absorption coefficient by Compton scattering: Amer. Mineral., 48, 1133-1143.

________. 1967. Estimation of mass absorption coefficient by Compton scattering: improvements and extensions of the method: Amer. Mineral., 52, 1493-1502.

Rucklidge, J. and Gasparrine, E.L. 1969. Electron microprobe analytical data reduction, EMPADR VII: Dept. Geol., Univ. of Toronto, 34p.

Sawkins, F.J. 1972. Sulfide ore deposits in relation to plate tectonics: Jour. Geology, 80, 377-397.

Schafer, H.N.S. 1966. The determination of iron (II) oxide in silicate and refractory materials- part I, a review: The Analyst, 91, 755-762.

Schilling, J.G. and Winchester, J.W. 1967. Rare-earch fractionation and magmatic processes, in Runcorn, S.K. (ed.), Mantle of the Earth and Terrestial Planets, Interscience Publ., London, 267-283.

Schnetzler, C.C. and Philpotts, J.A. 1970. Partition coefficients of REE between igneous matrix material and rock forming mineral phenocrysts--II, Geochem. Cosmochem. Acta, 34, 331-340.

Shaw, D.M. 1970. Trace element fractionation during anatexis, Geochim, Cosmochim, Acta, 34, 237-243.

Shimizu, N. 1974. Rare earth elements (REE) in garnets and clinopyroxenes from garnet lherzolite nodules in kimberlites, Carnegie Inst. Washington Yearb. 73, 954.

Sims, P.K. Precambrian tectonics and mineral deposits, Lake Superior region: Econ. Geol., 71, 1092-1127.

Sims, P.K. and Morey, G.B. 1972. Resume of geology of Minnesota: in Sims, P.K. and Morey, G.B. (eds.), Geology of Minnesota: A Centennial Volume, Minn. Geol. Survey, 3-17.

Skinner, B.J. and Peck, D.L. 1969. An immiscible sulfide melt from Hawaii: in Magmatic ore deposits; a symposium, Econ. Geol., Monograph, 4, 310, 322.

Snider, D.W., Klasner, J.S. Quam, S., Lilienthial, R., Geraci, P. and Grosz, A. 1977. Geophysical studies of peridotite dikes, Yellow Dog Plains, Northern Michigan (abs): 23rd. Ann. Meet. Institute Lake Superior Geology, Thunder Bay, Ont., May 2-8, 1977, p. 42.

Stanton, R.L. 1972. Ore Petrology, McGraw-Hill Book Co., New York, 713p.

Sweatman, T.R. and Long, J.V.P. 1969. Quantitative Electron-probe microanalysis of rock-forming minerals, Jour. Petrology, 10, 332-379.

Tilley, C.E. 1950. Some aspects of magmatic evolution, Geol. Soc. London, Quarterly Jour., 106, 37-61.

Van Schmus, W.R. 1976. Early and middle Proterozoic history of the Great Lakes area, North America, Phil. Trans. R. Soc. Lond. A., 280, 605-628.

Weiblen, P.W., Mathez, E.A. and Morey, G.B. 1972. Logan intrusions: in Sims, P.K. and Morey, G.B., Geology of Minnesota: A Centennial Volume, Minn. Geol. Survey, 394-406.

Weis, L.A. 1974. A petrochemical investigation of the Winona quadrangle basalts, Northern Michigan, M.S. Thesis, Univ. Toledo.

White, W.S. 1966. Tectonics of the Keweenawan basin, Western Lake Superior region, S.S. Geol. Soc. Prof. Paper 524-E, 23p.

________. 1972. Keweenawan flood basalts and Continental Rifting (abs): Geol. Soc. Amer. Abstracts with Programs, 4, 732-734.

Wilband, J.T. 1975. Rapid method for background corrections in trace element analysis by X-ray fluorescence: an extension of the Reynolds method, Amer. Mineral., 60, 320-323.

Wood, W.W. 1962. Distribution and stratigraphic position of Late Precambrian diabase dikes in parts of Northern Michigan, M.S. Thesis, Mich. St. Univ., 57p.

Wyllie, P.J. 1967. Ultramafic and Related Rocks: John Wiley and Sons, New York, 464p.

APPENDICES

APPENDIX A

Analytical Methods

X-ray fluorescence
Neutron activation
Electron microprobe
Titrametric

ANALYTICAL METHODS

Analytical methods used in this study include X-ray fluorescence, neutron activation, electron microprobe and titrametric analyses.

X-Ray Fluorescence

The equipment used in x-ray fluorescence analysis includes:

1. General Electric XRF x-ray generator and detector panel.
2. Flow-proportional counter with p-10 gas (90 percent argon - 10 percent methane) Helium path used when needed.
3. Analyzing crystals--LiF, ADP, PET.
4. High power Mo and Cu target tubes.
5. Other associated electronic equipment.

X-ray fluorescence analysis was used for whole rock analysis for the following elements: Fe, Ca, K, P, Si, Al, Mg, Mn, Cr, Cu, Ni and Zn. The latter four elements were determined after correcting for absorbtion by the Reynolds' method (Reynolds, 1963, 1967; Wilband, 1975). The sample preparation method used was a fusion technique using the proportions 1:14:3 for sample:flux:binder as used by Fabbi (1972). The phosphorous correction suggested by Fabbi (1971) was also used.

Neutron Activation Analysis

Neutron activation analysis was used to determine whole rock compositions for the rare-earth elements, La, Ce, Sm, Eu, Yb, and Lu and for Na, Cr, and Co. The equipment used in this analysis includes:

1. A Triga Mark I nuclear reactor.
2. A GeLi detector--a lithium drifted germanium crystal held at cryogenic temperatures by liquid nitrogen.
3. Multichannel analyzer, anphilication equipment and other associated electronics.

Powdered (1.00000 gram) rock samples, crushed to pass through a 200 mesh seive, were placed in polyvinal vials and sealed for irradiation and analysis. Gloves were used in sample handling to avoid contamination, particularly for Na. In the Na analysis samples and standards were irradiated for 15 minutes at a flux of 10^{12} neutrons/cm^2-sec. After Na analysis all samples were again irradiated for two hours at the same flux and analyzed for the remaining elements following the methods described by Gordon et al. (1972).

As previously mentioned, the samples were irradiated along with liquid standards of 1, 3, 5, and

10 ppm La and Sm as a check on the first results. Excellent agreement occurred between both sets of analyses (see Appendix B).

Chromium was determined by two methods, X-ray fluorescence and neutron activation analysis. Excellent agreement was obtained between both data sets (r = .98). The chromium results of both methods are listed in Appendix B. The Cr concentrations determined by neutron activation are 5 to 6 percent higher than those determined by x-ray fluorescence.

Electron Microprobe Analysis

Olivine, pyroxene, and feldspar mineral compositions were determined from carbon coated polished thin sections with an electron microprobe x-ray analyzer, Applied Research Laboratories Model EMX-SM.

The conditions for analysis were: 15 KV accelerating voltage for analyzing Si, Al, Mg, Ca, Na and Ti; 25 KV accelerating voltage for Fe, Mn, Cr, and Ni; beam current = 0.2 microamps; instrumental drift was corrected for by using constant current analyzing conditions, set so the counting time was near ten seconds; analysis took place under a focused point beam.

All the data collected on the electron microprobe were processed by the computer program EMPADR VII (Rucklidge, 1969) which reduces the raw data, applies the corrections suggested by Sweatman and Long (1968) and produces a final analysis in terms of standard oxides.

An average of five different points were analyzed on each mineral with each point counted twice. The correction program used the mean of these analyses to determine the oxide composition of olivine and pyroxenes, little zoning was evident in the analyzed samples. The anorthite content of the plagioclase feldspars was determined by measuring Ca, Na, and Si.

Titrametric Analysis

A titrametric method described by Weis (1974) modified after Schafer (1966) was used for the determination of ferrous iron in the analyzed samples. The method used to determine the loss on ignition for analyzed samples was modified after a procedure used in the Chemical Laboratories of the Geology Division of the Research Council of Alberta (Weis, 1972). For detailed procedures of these methods see Weis (1974).

Table 6.--Comparative standards used in the analyses.[*]

X-ray Fluorescence	
W-1	BCR-1
G-2	AGV-1
G-1	GSP-1
PCC-1	DTS-1
NBS-1a	NBS-177
Neutron Activation	
W-1	BCR-1
G-2	AGV-1
PCC-1	GSP-1
liquids 1, 3, 5, 10 ppm La and Sm	
Electron Microprobe	
Element	Standard
Si	Quartz, Albite
Al	Al_2O_3 glass
Ca	Wollastonite, Anorthite
Ti	Rutile
Fe	Hematite, Pure Iron
Ni	Pure Nickel Metal
Cr	Pure Chromium Metal
Mn	Pure Manganese Metal
Na	Albite
Titrametric	
W-1 DTS-1	

[*] Flanagan's (1973) concentrations were used.

APPENDIX B

Whole Rock Compositions

Yellow Dog Plains Peridotite and Diabase Dikes

Whole Rock Analyses.

Sample No.	SiO2	Al_2O_3	Fe_2O_3	FeO	MgO	CaO	Na_2O	K_2O	LOI	TiO_2	P_2O_5	MnO	Total
Peridotite													
YDPLO	40.71	4.15	6.77	7.84	26.09	3.52	.46	.24	8.03	.87	.11	.18	98.97
YDPOO	44.45	4.46	5.35	8.47	23.25	5.67	.62	.25	5.58	.79	.10	.19	99.18
YDP 1	41.18	5.08	6.15	7.77	25.79	4.01	.56	.26	8.18	.54	.08	.17	99.77
YDP 2	42.18	3.83	5.44	8.58	26.97	3.57	.42	.24	7.19	.56	.11	.18	99.27
YDP 4	42.67	4.18	6.44	8.33	27.50	3.69	.48	.23	7.06	.70	.10	.19	101.57
YDP11	42.73	4.16	6.21	8.12	25.94	4.03	.52	.24	6.76	.73	.10	.18	99.72
YDP18	43.51	5.33	5.47	8.77	24.09	5.43	.89	.25	5.56	.88	.12	.19	100.49
YDP22	43.51	4.92	4.64	9.70	25.82	5.12	.54	.28	5.92	.84	.11	.19	101.59
YD222*	42.94	4.85	6.26	8.72	24.80	4.92	.55	.29	5.45	.82	.11	.18	99.89
YDP26	42.33	5.14	6.04	8.16	25.14	4.73	.73	.25	6.33	.83	.11	.18	99.97
YDP28	41.54	3.94	6.66	8.06	26.00	4.40	.49	.17	7.31	.63	.08	.19	99.47
YD282*	42.25	3.52	7.22	7.68	27.36	4.10	.46	.29	7.26	.67	.09	.19	101.09
YDP30	42.84	3.69	5.56	8.59	25.44	3.51	.48	.22	7.73	.64	.09	.19	98.98
2M2*	41.27	3.74	6.47	7.89	25.15	3.67	.55	.27	7.50	.72	.10	.18	97.51
2M	42.32	4.26	6.61	7.89	25.15	3.84	.55	.24	7.50	.76	.09	.17	99.38
4M	42.43	4.50	5.87	8.14	26.20	4.10	.53	.23	6.96	.77	.09	.19	100.01
8M	42.13	3.94	4.54	9.46	27.70	4.70	.44	.23	6.00	.67	.09	.19	100.09
12M	41.82	4.18	5.24	8.84	26.47	4.14	.32	.24	6.59	.70	.10	.19	98.83
16M	43.20	4.02	5.23	8.88	25.86	4.45	.34	.21	7.04	.63	.09	.19	100.14
20M	41.16	4.35	4.35	9.87	27.67	3.83	.20	.23	6.89	.68	.10	.19	99.52
24M	42.87	3.58	4.62	9.90	27.11	3.89	.45	.24	6.11	.62	.09	.19	99.67
28M	42.05	3.58	5.14	9.70	28.26	3.71	.39	.22	6.28	.65	.09	.19	100.26
32M	43.22	3.69	4.50	10.21	27.46	3.82	.37	.21	6.15	.65	.09	.20	100.57
Diabases													
ZPK-1	51.32	13.52	2.36	11.05	3.98	7.11	2.37	1.69	2.86	2.47	.30	.18	99.21
ZPK-2	51.91	13.42	2.83	10.72	3.56	6.57	2.92	1.91	3.39	2.59	.33	.17	100.32
LHP	50.94	14.70	4.49	8.13	5.70	9.70	2.36	.39	2.24	1.75	.20	.25	100.85
WL	49.97	12.60	4.58	10.32	7.07	8.20	2.43	.79	1.29	3.33	.38	.26	101.72
WL2*	49.97	12.90	3.59	11.12	7.37	8.50	2.53	.84	1.29	3.43	.38	.26	102.18
PKD	50.40	14.36	2.00	7.18	12.19	11.77	1.70	.45	1.56	.50	.03	.15	102.29
LM-2	50.08	13.89	2.74	11.44	4.06	7.61	2.38	1.41	2.74	2.65	.24	.16	99.40
KDS	53.14	14.48	3.09	10.69	6.37	3.51	1.87	.89	2.45	1.69	.15	.22	98.55

*Duplicate Analyses

Trace and Rare-Earth Element Concentrations (PPM).

Sample No.	Ni	Cr	Zn	Cu	Mn	Co	Cr^1	La	Ce	Sm	Eu	Yb	Lu	La^2	Sm^2
							Peridotite								
YDP LO	1401	2376	104	101	1310	126	1852	3.95	19	2.14	.93	.58	.14	5.52	2.28
YDP OO	1494	2121	97	101	1170	130	2258	2.84	20	2.10	.66	.69	.17	5.92	2.45
YDP 1	1314	2363	85	95	1360	132	2139	1.34	9	1.35	.54	.73	.18	4.11	1.56
YDP 2	1431	2606	99	99	1420	136	2280	2.72	23	1.92	.79	.73	0.00	6.19	2.13
YDP-11	1402	2443	95	102	1360	130	2485	4.36	18	1.91	.75	.21	.15	5.99	1.91
YDP-18	1434	2327	93	98	1230	124	2286	6.61	18	2.12	1.13	.57	.16	7.92	2.12
YDP-22	1462	2411	100	145	1900	149	2185	4.36	14	2.07	.84	.96	.20	5.65	2.34
YDP222*	1428	2173	96	147	1855	125	2133	5.25	16	2.20	.85	.90	.18	4.98	2.51
YDP-26	1432	2548	92	100	1250	117	2328	3.39	16	2.20	.81	1.06	.16	5.92	2.46
YDP-28	1460	2421	107	100	1340	128	2394	3.40	15	1.55	.74	.57	.20	4.27	1.55
YDP282*	1437	2421	95	100	1345	133	2355	1.02	16	1.53	.74	1.18	.11	3.32	1.69
YDP-30	1387	2716	94	99	1440	116	2348	3.49	14	1.83	.93	.88	.21	2.55	2.11
2M	1347	2495	96	100	1415	133	2447	4.34	18	2.19	1.02	.13	.20	5.02	2.19
4M	1448	2471	90	100	1355	123	2505	4.82	11	2.03	.85	.57	.16	6.20	2.32
8M	1441	2639	95	98	1395	116	2521	1.80	12	1.87	.79	1.08	.17	4.00	2.02
12M	1495	2739	88	99	1380	128	2420	2.48	17	2.04	.79	.40	.18	5.96	1.64
16M	1451	2798	90	102	1435	123	2535	1.27	14	1.87	.57	.56	.18	5.75	1.97
20M	1486	2848	98	98	1450	131	2773	2.94	14	1.81	.82	1.12	.13	5.78	2.15
24M	1474	2740	92	102	1455	129	2631	3.67	25	1.72	.76	.67	.09	6.24	2.00
28M	1477	2823	94	99	1495	140	2806	4.59	17	1.81	.86	.88	.09	5.32	1.95
32M	1513	2853	93	102	1510	134	2645	2.20	15	1.75	.62	.32	.18	5.99	1.79
							Diabase Dikes								
ZPK-1	1332	0	120	95	0	45	52	24.8	44	7.28	2.25	1.91	.36	21.6	7.38
ZPK-2	1292	0	121	95	0	43	32	24.8	48	7.74	2.41	3.34	.56	21.5	8.13
LHF	1941	660	95	143	150	59	169	9.97	28	4.92	1.74	2.40	.56	11.5	5.35
WL	2026	0	124	174	0	46	125	25.4	48	7.13	2.78	3.58	.69	25.8	10.13
PKD	1195	413	42	106	240	50	312	.74	45	1.35	.95	1.75	.54	1.84	1.39
LM-2	1270	0	110	97	0	45	66	13.5	40	6.30	2.13	1.49	.67	21.3	6.66
KDS	1694	161	102	119	30	55	219	10.7	25	4.83	1.41	1.59	.47	17.4	5.20

*Duplicated Analyses.

[1] CR Determined by X-Ray Fluorescence.

[2] La and Sm analyses with liquid standards.

APPENDIX C

Mineral Compositions of the Yellow Dog Plains Peridotite

Olivines
Clinopyroxenes
Orthopyroxenes

YDPP Clinopyroxene Compositions.

ID	SiO_2	Al_2O_3	TiO_2	CaO	MgO	FeO*	NiO	Cr_2O_3	MnO	Total	Wo	En	Fs
4M1	51.78	2.58	1.25	19.41	16.56	6.85	.11	.53	.20	99.26	40.62	48.19	11.18
4M2	51.97	2.12	.78	18.76	17.79	6.87	.11	.81	.20	99.41	38.39	50.64	10.97
4M4	51.18	2.67	1.16	19.09	16.74	6.83	.10	.66	.20	98.63	40.01	48.81	11.18
6M3	52.55	2.27	.54	18.80	17.41	6.65	.10	.84	.17	99.32	38.99	50.24	10.77
6M2	51.90	2.44	1.07	19.30	16.21	6.90	.10	.70	.21	98.83	40.86	47.74	11.40
6M1	52.52	2.04	.49	17.98	18.34	6.38	.13	.91	.20	98.97	37.10	52.62	10.28
8M2	53.10	2.12	.55	18.22	18.31	6.15	.10	.95	.17	99.67	37.57	52.53	9.90
12M1	51.95	2.06	.54	18.86	17.91	6.42	.15	.87	.17	98.93	38.66	51.06	10.27
14M1	50.26	2.85	1.05	18.52	17.08	7.37	.14	.55	.21	98.03	38.56	49.47	11.97
16M1A	52.05	1.69	.49	17.69	18.86	6.34	.13	.90	.18	98.32	36.19	53.68	10.13
16M3	52.09	1.82	.43	17.31	18.93	6.33	.13	.87	.18	98.09	35.62	54.20	10.18
18M1	51.77	2.51	.72	18.68	17.40	7.10	.06	.86	.15	99.26	38.58	49.98	11.44
22M1	52.07	2.94	.98	18.71	17.12	6.61	.10	.79	.18	99.51	39.23	49.94	10.82
22M2	52.43	2.22	1.06	19.23	16.61	6.90	.12	.50	.23	99.28	40.29	48.41	11.29
26M1	52.10	2.42	1.19	19.23	16.59	6.54	.12	.46	.18	98.82	40.56	48.69	10.75
28M1	52.79	2.28	.53	17.86	18.15	6.80	.14	1.02	.20	99.76	36.89	52.15	10.96
28M2	52.46	2.75	.80	17.81	17.14	6.89	.12	.95	.18	99.10	37.87	50.69	11.44
32M1	54.08	1.59	.43	18.15	17.52	6.71	.12	.99	.18	99.76	38.01	51.03	10.96
32M2A	54.48	1.68	.44	18.83	17.98	6.39	.14	.85	.24	101.03	38.55	51.22	10.22
32M3	54.35	1.48	.44	18.36	17.58	6.30	.12	.95	.18	99.77	38.46	51.23	10.30

*Total Fe as FeO.

YDPP Olivine Compositions.

ID	SiO_2	FeO*	MgO	CaO	MgO	NiO	Cr_2O_3	Total	Fo
4M1	38.98	19.47	41.54	.13	.24	.37	.03	100.77	79.18
4M2	39.89	19.26	42.02	.10	.23	.34	.02	101.86	79.54
4M3	38.27	19.25	41.94	.11	.21	.33	.02	100.13	79.36
6M1	39.31	18.73	42.17	.20	.24	.41	.03	101.09	80.06
6M2	38.82	17.89	41.98	.26	.24	.38	.04	99.61	80.70
6M3	39.09	18.98	41.88	.20	.23	.43	.04	100.85	79.72
8M1	38.58	19.06	41.64	.23	.26	.44	.05	100.26	79.57
8M2	38.51	19.86	41.81	.23	.26	.44	.04	101.15	78.96
8M3	39.19	17.87	42.40	.57	.22	.44	.07	100.76	80.88
12M1	38.50	19.38	41.74	.24	.28	.38	.03	100.55	79.33
12M2	38.51	19.01	42.07	.30	.26	.42	.03	100.60	79.78
12M3	38.80	19.16	40.99	.29	.28	.39	.03	99.94	79.22
12M4	37.54	19.18	41.15	.25	.29	.47	.03	98.91	79.27
14M1	39.65	19.13	41.03	.11	.27	.49	.04	100.72	79.26
14M2	37.77	19.38	40.92	.16	.24	.40	.03	98.90	79.00
14M3	38.42	19.69	41.06	.16	.26	.41	.03	100.03	78.80
16M1	39.30	17.35	41.12	.35	.25	.29	.03	98.69	80.86
16M2	39.37	16.61	42.69	.45	.24	.31	.05	99.72	82.08
16M3	39.35	17.50	41.89	.29	.25	.32	.02	99.62	81.01
18M1	39.81	17.04	42.67	.26	.27	.35	.05	100.45	81.69
18M2	39.41	17.05	42.72	.19	.27	.35	.03	100.02	81.70
18M3	38.00	16.75	42.40	.31	.25	.24	.06	98.01	81.85
22M1	39.79	17.53	41.93	.23	.25	.36	.03	100.12	81.00
22M2	39.29	17.43	41.80	.22	.25	.38	.03	99.40	81.03
22M3	39.58	17.81	41.78	.31	.23	.39	.05	100.15	80.70
26M1	39.37	17.62	41.65	.25	.24	.36	.04	99.53	80.82
26M2	39.58	17.05	41.98	.28	.24	.37	.04	99.54	81.44
26M3	39.40	17.40	41.36	.25	.25	.35	.04	99.04	80.90
28M1	37.42	18.26	42.41	.43	.22	.40	.04	99.18	80.54
28M2	39.70	17.34	41.91	.18	.18	.29	.05	99.65	81.16
28M4	39.29	18.69	41.67	.19	.23	.36	.03	100.46	79.89
32M1	39.23	17.36	42.32	.29	.26	.35	.04	99.85	81.26
32M2	39.09	17.36	42.34	.21	.23	.27	.07	99.57	81.27
32M3	39.13	15.76	43.02	.29	.24	.30	.05	98.79	82.94

*Total Fe as FeO.

YDPP Orthopyroxene Compositions.

ID	SiO_2	Al_2O_3	TiO2	CaO	MgO	FeO*	NiO	Cr_2O_3	MnO	Total	Wo	En	Fs
8M1	54.40	1.82	.43	2.14	28.98	11.32	.12	.50	.26	99.90	4.17	78.61	17.23
12M3	54.30	1.37	.60	1.77	29.12	12.19	.10	.25	.24	99.95	3.42	78.20	18.38
12M4	54.89	1.38	.55	1.90	28.91	11.70	.11	.29	.23	99.97	3.70	78.48	17.82
14M2	54.93	1.29	.66	1.59	28.96	12.20	.13	.20	.27	100.24	3.10	78.37	18.52
14M3	54.16	1.32	.59	1.87	29.27	12.25	.13	.39	.28	100.25	3.59	78.08	18.34
16M2	53.05	1.92	.46	1.74	30.07	11.54	.15	.37	.26	99.58	3.30	79.56	17.14
18M4	55.19	1.77	.47	1.94	28.88	11.99	.09	.49	.28	101.10	3.76	78.07	18.17
26M2	54.50	1.48	.55	1.72	28.61	11.81	.15	.36	.27	99.45	3.38	78.46	18.16
28M3	55.14	1.95	.45	1.91	28.73	11.62	.14	.45	.27	100.67	3.75	78.44	17.80
32M2B	55.84	1.77	.38	2.02	28.50	11.57	.14	.53	.16	100.91	3.98	78.21	17.81

*Total Fe as FeO.